April 2021

Enhancing flat plate heat convection using a pair of winglets – The effect of transverse spacing

Siddharth Koushik Mohanakrishnan
University of Windsor, mohanak@uwindsor.ca

Enhancing flat plate heat convection using a pair of winglets – The effect of transverse spacing

By

Siddharth Koushik Mohanakrishnan

A Major Research Paper
Submitted to the Faculty of Graduate Studies
through the Department of Mechanical, Automotive and Materials Engineering
in Partial Fulfillment of the Requirements for
the Degree of Master of Applied Science
at the University of Windsor

Windsor, Ontario, Canada

2021

Enhancing flat plate heat convection using a pair of winglets – The effect of transverse spacing

by

Siddharth Koushik Mohanakrishnan

APPROVED BY:

_____

S. Ray
Essex Energy

_____

V. Roussinova
Department of Mechanical, Automotive and Materials Engineering

_____

D. Ting, Advisor
Department of Mechanical, Automotive and Materials Engineering

January 05, 2021

DECLARATION OF CO-AUTHORSHIP/PREVIOUS PUBLICATION

I. Co-Authorship

I hereby declare that this major research paper incorporates material that is result of joint research, as follows:

Chapter 2 of the major research paper was co-authored with Dr. Yang Yang and Mr. Steve Ray under the supervision of professor Dr. David Ting. In all cases, the key ideas, primary contributions, experimental designs, data analysis, interpretation, and writing were performed by the author, and the contribution of co-authors, Dr. Yang Yang, Mr. Steve Ray, and Dr. David Ting was primarily through the provision of feedback on refinement of ideas and editing of the manuscript, etc...

I am aware of the University of Windsor Senate Policy on Authorship and I certify that I have properly acknowledged the contribution of other researchers to my major research paper and have obtained written permission from each of the co-author(s) to include the above material(s) in my thesis.

I certify that, with the above qualification, this thesis, and the research to which it refers, is the product of my own work.

II. Previous Publication

This major research paper includes 1 original paper that has been co-authored and submitted for publication in peer reviewed journals, as follows:

Thesis Chapter	Publication title/full citation	Publication status*
Chapter 2	*Siddharth Koushik Mohanakrishnan, Yang Yang, David S-K. Ting, and Steve Ray., The effect of transverse spacing of a winglet pair on flat plate heat convection.*	*Submitted*

I certify that I have obtained a written permission from the copyright owner(s) to include the above published material(s) in my thesis. I certify that the above material describes work completed during my registration as a graduate student at the University of Windsor.

III. General

I declare that, to the best of my knowledge, my thesis does not infringe upon anyone's copyright nor violate any proprietary rights and that any ideas, techniques, quotations, or any other material from the work of other people included in my thesis, published or otherwise, are fully acknowledged in accordance with the standard referencing practices. Furthermore, to the extent that I have included copyrighted material that surpasses the bounds of fair dealing within the meaning of the Canada Copyright Act, I certify that I have obtained a written permission from the copyright owner(s) to include such material(s) in my thesis.

I declare that this is a true copy of my thesis, including any final revisions, as approved by my thesis committee and the Graduate Studies office, and that this thesis has not been submitted for a higher degree to any other University or Institution.

ABSTRACT

We can manipulate the prevailing atmospheric wind to enhance the convective cooling of a solar photovoltaic panel and thus its energy conversion efficiency. The transverse spacing (D) of a delta winglet pair was examined for its role in convective heat transfer enhancement. A pair of winglets with an inclination angle of 90° and chord/height (c/h) ratio of 2 was positioned at an attack angle of 30° with respect to incoming wind at a Reynolds number, based on the winglet height, of 6300. The transverse distance, D, was varied from 0 to 3h in 1h increments. The Nusselt number normalized by the reference no-winglet case, Nu/Nu_0, was determined from the surface temperature measured by a thermal camera. The D=2h case was found to lead to the largest Nu/Nu_0. This significant heat transfer enhancement was explained in terms of vortical flow characteristics detailed at 10h downstream of the winglet pair, where the most potent downwash was induced when D=2h.

DEDICATION

I dedicate this major research paper to my beloved parents Mr. Mohanakrishnan Subramanian, Mrs. Geetha Mohanakrishnan and my sister Dr. S. M. Anusha.

ACKNOWLEDGEMENTS

First and foremost, I would like to thank Dr. David S.-K. Ting for his supervision, valuable suggestions and guiding me throughout my journey in this program. I thank Mr. Steve Ray for his contributions and support. I also thank Dr. Vesselina Roussinova in providing valuable time in shaping up my work. I would like to thank Mr. Andy Jenner and Mr. Bruce Durfy for their technical assistance.

This work was made possible by the Natural Sciences and Engineering Research Council of Canada and the Ontario Centers of Excellence.

TABLE OF CONTENTS

LIST OF TABLES

LIST OF FIGURES

NOMENCLATURE

A	Local heat transfer area (mm^2)
B	Bias uncertainty
c	Chord length of the winglet (mm)
D	Transverse distance between the trailing edges of the winglet pair (mm)
H	Convective heat transfer coefficient
h	Winglet height (mm)
k_{PTFE}	Conductivity of the plate (W/m·K)
N	Sampling number
Nu	Nusselt number
Nu_0	Unperturbed reference Nusselt number
P	Precision uncertainty
$PTFE$	Polytetrafluoroethylene
$\dot{Q}_{convection}$	Convective heat transfer rate (W)
$\dot{Q}_{radiation}$	Radiative heat transfer rate (W)
$\dot{Q}_{Total}$	Total heat transfer rate (W)
Re_h	Reynolds number based on the winglet height
std_j	Standard deviation of studied individual parameters
std_y	Standard deviation of the dependent variable (Nu/Nu_0)
T_{Air}	Surrounding air temperature (K)

T_{Bottom}	Bottom surface temperature (K)
T_{Top}	Top surface temperature (K)
T_{Wall}	Wall temperature (K)
Tu	Stream-wise turbulence intensity
u_{rms}	Root-mean-square velocity in the X direction (m/s)
v_{rms}	Root-mean-square velocity in the Y direction (m/s)
w_{rms}	Root-mean-square velocity in the Z direction (m/s)
u_i	Instantaneous fluctuating velocity in the X direction (m/s)
U_i	Instantaneous velocities in the X direction (m/s)
$\bar{U}$	Time-averaged local velocity in the X direction (m/s)
U_∞	Time-averaged free-stream velocity (m/s)
v_i	Instantaneous fluctuating velocity in the Y direction (m/s)
V_i	Instantaneous velocities in the Y direction (m/s)
$\bar{V}$	Time-averaged velocity in the Y direction (m/s)
w_i	Instantaneous fluctuating velocity in the Z direction (m/s)
W_i	Instantaneous velocities in the Z direction (m/s)
$\bar{W}$	Time averaged velocity in the Z direction (m/s)
X	Streamwise direction
Y	Widthwise direction
Z	Vertical direction

Greek Symbols

α	Attack angle of the winglet (degrees)
β_j	Regression coefficient
β_j^{std}	Standardised regression coefficient
ε	Emissivity
λ	Taylor micro-scale (m)
Λ	Integral scale (m)
τ	Autocorrelation factor
τ_λ	Taylor time scale (s)
τ_Λ	Integral time scale (s)
ω	Vorticity (s^{-1})
Ω	Non-dimensional vorticity

CHAPTER 1

INTRODUCTION

1.1 Motivation and Background

Solar photovoltaics (PV) is a promising renewable energy technology [1] and it is considered as the best source to make a revolution in energy field [2]. A major challenge is that its energy conversion efficiency drops substantially in the summer due to increased cell temperature [3]. This increased cell temperature reduces the efficiency of PV panels [4]. The cell temperature can be reduced by either deploying active or passive methods of cooling. Some of the active cooling methods involve liquid immersion, concentrating photovoltaic thermal system, jet impingement cooling, thermophotovoltaic system [5]. Among these, liquid immersion, and jet impingement appear to be the best active cooling technologies cited in the literature [6]. However, all these methods involve the use of additional mechanical equipment and electrical power to force water on the surface of photovoltaics [7]. So, an alternative option of using passive method using vortex generators to cool the PV panels can be adapted to eliminate the use of additional equipment and electric power.

Among the types of vortex generators, delta winglets seem to be effective when it comes to convective heat transfer because of their ability to generate long-lasting vortices [8]. Most of the studies related to delta winglets were conducted inside a confined space. To better understand the longitudinal vortices created by the delta winglets, it is fundamental to investigate the role of delta winglets over an unconfined flat surface.

1.2 Major Paper Objective and Overview

The objective of this study is to investigate the role of delta winglets on heat transfer enhancement from an unconfined flat plate with varying transverse distance between the trailing edges of the delta winglets. The heat transfer measurement was captured using thermal camera and flow was measured using triple probe hot-wire anemometer system. The content in different chapters is briefed as follows.

Chapter 1 (Introduction)

The motivation, background, major paper objective and overview are given in this chapter.

Chapter 2

This chapter experimentally investigates the role of the transverse distance between the trailing edges of the winglet pair (D=0, D=1h & D=2h) at Re_h=6300 on heat transfer and flow characteristics. The chosen winglet attack angle is 30°, and chord length and height are 30 mm and 15 mm respectively leading to the aspect ratio (c/h) of 2. First the investigation of the role of transverse distance (D) between the trailing edges of the winglet pair on heat transfer for four cases, D=0, D=1h, D=2h, and D=3h is discussed. Then the flow characteristics are delineated for three cases of transverse distance between the trailing edges of the winglet pair viz, D=0, 1h and 2h with the help of hot-wire measurement. Next the results of multiple linear regression are discussed which correlates the impact of influential flow properties with the heat transfer enhancement.

Chapter 3 (Conclusion)

This final chapter summarises the results from the last chapter. It also brings forth some recommendations for future study.

Appendix A.

This section details the uncertainty analysis involved in the studied parameters.

Appendix B.

This section compares the streamwise, spanwise and height wise turbulent intensities and their respective influence on heat transfer.

Appendix C.

The impact of all the flow parameters on heat transfer is documented in this section, supporting the regression analysis conveyed in Chapter 2, Section 2.4.3.

Appendix D.

This section discusses some non-ideal real wind effects on the proposed winglets model.

Appendix E.

This section discusses the scaling factor of the winglets from the wind tunnel model to a real PV panel (array).

References

[1] Rosenbloom, D., Meadowcroft, J. (2014). Harnessing the Sun: Reviewing the potential of solar photovoltaics in Canada. Renewable and Sustainable Energy Reviews, 40, 488–496.

[2] Vinoth Kanna, I., Pinky, D. (2020). Solar research–a review and recommendations for the most important supplier of energy for the earth with solar systems. International Journal of Ambient Energy, 41(8), 962–968.

[3] Teo, H. G., Lee, P. S., Hawlader, M. N. A. (2012). An active cooling system for photovoltaic modules. Applied Energy, 90 (1), 309-315.

[4] Rabie, R., Emam, M., Ookawara, S., Ahmed, M. (2019). Thermal management of concentrator photovoltaic systems using new configurations of phase change material heat sinks. Solar Energy, 183, 632–652.

[5] Bayrak, F., Oztop, H. F., Selimefendigil, F. (2020). Experimental study for the application of different cooling techniques in photovoltaic (PV) panels. Energy Conversion and Management, 212, 112789.

[6] Jakhar, S., Soni, M. S., Gakkhar, N. (2016). Historical and recent development of concentrating photovoltaic cooling technologies. Renewable and Sustainable Energy Reviews, 60, 41-59.

[7] Maleki, A., Haghighi, A., El Haj Assad, M., Mahariq, I., & Alhuyi Nazari, M. (2020). A review on the approaches employed for cooling PV cells. Solar Energy, 209, 170–185.

[8] Arianmehr, I., Ting, D. S. K., Ray, S. (2013). Assisted turbulence convective heat transfer for cooling the photovoltaic cells. ASME 2013, Heat Transfer Summer Conf.

Collocated with the ASME 2013 7th International Conference on Energy Sustainability and the ASME 2013 11th International Conference on Fuel Cell Science, Engineering and Technology, Minnesota, United States of America, Publisher: New York : American Society of Mechanical Engineers, 1-10.

CHAPTER 2

ENHANCING FLAT PLATE HEAT CONVECTION USING A PAIR OF WINGLETS – THE EFFECT OF TRANSVERSE SPACING

Siddharth Koushik Mohanakrishnan [a], Yang Yang [a], David S-K. Ting [a], and Steve Ray [b]

[a] Turbulence and Energy Laboratory, University of Windsor, ON, Canada

[b] Essex Energy, Oldcastle, ON, Canada

2.1 Introduction

Solar photovoltaics (PV) is a promising renewable energy technology [1] and the best source to revolutionize the energy field [2]. A major challenge is that its energy conversion efficiency decreases notably with increasing cell temperature [3, 4]. To mitigate this, we can employ different means to cool the PV panel. The various cooling methods can be categorized into active and passive cooling methods. Active cooling methods include liquid immersion and jet impingement, among others [5, 6]. These active methods, however, require additional mechanical equipment and external power input, thus increasing their cost and maintenance requirements [7]. The passive approach, on the other hand, eliminates the complication of additional equipment and power input.

Passively cooling the PV panels using turbulent generators is a promising means to promote heat convection [8]. Among these, many vortex generators have been designed to spawn vortices to scoop away the thermal energy [9], and winglets are particularly promising in creating streets of vortices that can survive far downstream [10]. Table 2.1 highlights studies of different types of turbulent generators. Wu et al. [10] examined the effect of a single delta winglet's attack angle over a flat surface and witnessed an escalation in turbulence with increasing attack angle from 30° to 60°. The

increase in attack angle contributed to heat transfer enhancement. da Silva et al. [11] conducted numerical study on three angles of attack (15°, 30° & 45°) for rectangular and delta winglets on a flat plate under three Reynolds numbers, 300, 600, and 900. Increasing Reynolds number resulted in increasing Nusselt number and at Reynolds number of 900, the Nusselt number enhancement increased from 40% to 68% when the attack angle was increased from 15° to 45°. The best ratio between heat transfer enhancement and pressure drop penalty was verified for a delta winglet vortex generator with an attack angle of 30° at Reynolds number of 600 and 900. Naik et al. [12] studied the spacing effect of the rectangular winglet pair on heat transfer enhancement over a flat plate. The 1*h*-spaced winglet pair led to higher heat transfer rate compared to 2*h*- and 3*h*-spaced winglet pairs.

Table 2.1. Highlight of studies on turbulent generators on heat transfer enhancement.

External Forced Convection	
Study & Generator Type	Studied parameters & Major findings
Wu et al. [10] Delta winglet	Attack angle: 30° to 60°. Heat transfer rate increases with increase in attack angle.
da Silva et al. [11] Rectangular & Delta winglets	Attack angle: 15°, 30°, & 45°. The rectangular winglet with an attack angle of 45° led to larger Nusselt number. The delta winglet with an attack angle of 30° resulted in the best heat transfer and pressure penalty ratio.
Naik et al. [12] Rectangular winglet pair	Spacing: 1*h*, 2*h*, & 3*h*. 1*h*-spaced winglet pair led to better heat transfer compared to 2*h*- and 3*h*-spaced winglet pairs.

Internal Forced Convection	
Study & Generator Type	Studied parameters & Major findings
Lei et al. [13] Delta winglet	Attack angle: 10° to 50° & Aspect ratio: 1 to 4. The heat transfer coefficient increases with increasing attack angle and aspect ratio.
Wijayanta et al. [14] Delta wing	Attack angle: 30° to 70°. The heat transfer rate is highest for attack angle of 70°.
Hiravennavar et al. [15] Delta winglet pair	Number of winglets: 1 & 2. The heat transfer rate enhanced by a winglet pair is more than that augmented by a single winglet.
Althaher et al. [16] Delta winglet	Number of winglets: 1, 2, & 3. Heat transfer performance increases with increase in the number of winglets.
Tang et al. [17] Rectangular & Delta winglets	Delta winglet pair with common-flow-up configuration provided better heat transfer performance.
Sinha et al. [18] - Rectangular winglet	Configuration: Inline and staggered row of tubes. The heat transfer performance of inline tubes configuration is better than staggered row of tubes.

Among the internal forced convection studies, Lei et al. [13] performed a numerical simulation on hydrodynamics and heat transfer of delta winglets in a fin-and-tube heat exchanger. They studied the effects of attack angles from 10° to 50° and aspects ratios from 1 to 4. Both heat transfer coefficient and friction factor increased with

increase in attack angle and aspect ratio. The heat transfer coefficient also increased with Reynolds number. They concluded that an attack angle of 20° along with an aspect ratio of 2 provided the best Colburn j-factor to friction factor ratio. Wijayanta et al. [14] numerically studied the heat transfer enhancement of a tube heat exchanger fitted with punched delta winglet vortex generators. They varied the attack angle of the delta winglets from 30° to 70° and found that at an attack angle of 70°, the Nusselt number, friction factor and thermal performance factor increased by 269%, 10.1 times and 1.1 times, respectively, compared to that of the smooth tube.

Hiravennavar et al. [15] conveyed that a pair of winglets doubled the heat transfer rate in a channel compared to a single winglet. Althaher et al. [16] explored the roles of Reynolds number, number of delta winglets, angle of attack and vortex generator geometry in a triangular duct. The Nusselt number increased as the number of delta winglets pair increased from 1 to 3, and the friction factor increased drastically with increasing attack angle from 18° to 50°.

Many studies also explored the specific shapes of winglets. Tang et al. [17] used field synergy principle to compare the heat transfer performance of rectangular and delta winglets pair in a rectangular channel. At a given Reynolds number, the delta winglet pair contributed to larger Nusselt number than its rectangular counterpart. Moreover, common-flow-up configuration led to a larger Nusselt number than the common-flow-down one. Sinha et al. [18] compared the effect of attack angle on two different configurations, inline tubes, and a staggered row of tubes, in a heat exchanger with rectangular winglet pairs. The performance of heat exchanger for inline tubes

configuration improved in terms of Nusselt number, friction factor and quality factor with decreasing attack angle from 165° to 160°.

It is thus clear that some subtle changes of a delta winglet can lead to significant variation in the resulting heat transfer rate. While many studies have focused on the attack angle, dimensions and shape of a winglet and a winglet pair, very few studies explored the effect of the spacing between a pair of winglets. Pourhedayat et al. [19] conducted a numerical study on the lateral spacing between a winglet pair on the heat transfer rate inside a circular tube with a diameter, D, of 47 mm. Both chord length and height of the winglets were 0.43D and winglet-winglet spacing of 0, 0.43D and 0.86D were studied. They found that the 0.43D-spaced pair resulted in the maximum heat transfer augmentation.

Most of the convection enhancement studies have been performed inside a confined space, and investigations on winglets such as [20, 21] are no exception. While confined flow represents internal forced convection, the interactions between the perturbed flow and the channel confinement are rather complex and particular to the specific tested conditions. To overcome this complication, Wu et al. [10] studied forced convection augmentation induced by a delta winglet over a largely unconfined flat surface. This study extends the investigation to uncover the effect of the spacing between a pair of side-by-side delta winglets.

2.2 Experimental Setup

The studied winglets, fashioned from 0.1 mm thick aluminium (1145-H19) sheet, are illustrated in Figure 2.1. Over the range of their studied conditions, Wu et al. [10]

found that a single winglet with an attack angle of 30° led to the highest heat transfer enhancement. In another study, an optimal aspect ratio of 2 was suggested by Lei et al. [13]. Accordingly, the winglets studied in this study were 15 mm high with a chord length of 30 mm, and they were placed at 30° with respect to the flow. The uniform flow in the wind tunnel was set at 7 m/s, leading to a Reynolds number based on the winglet height of 6.3×10^3.

The winglet pair was fixed to the top surface of a 3 mm thick, 295 mm wide and 380 mm long *PTFE* (Polytetrafluoroethylene) plate inside a wind tunnel of 76 cm × 76 cm cross-section as shown in Figure 2.2. The conductivity and emissivity of the plate are 0.25 $Wm^{-1}K^{-1}$ [22] and 0.92 [23], respectively. The bottom surface of the *PTFE* plate was heated by steam continuously generated in a water bath, maintaining the bottom surface of the plate at 100°C. The temperature of the top surface was measured by a FLIR C2 thermal camera. The thermal camera with 60 by 80-pixel resolution was positioned at 0.5 m above the heated plate. The orthogonal coordinates X, Y, and Z represent stream-wise, width-wise and height-wise directions, respectively. The origin O was defined as the midpoint of the gap at the leading edge of the winglet pair; see Figure 2.1. The vortical flow reached a slowly-decaying, quasi-steady condition between 5*h* and 10*h* downstream of the winglet pair. Therefore, the turbulent flow characteristics generated by the delta-winglet pair over the unheated *PTFE* plate were measured at 10*h* (150mm) downstream of the leading edge of the winglet pair. We used a 3D hotwire (type 55P95) and a constant temperature anemometer for this purpose. The turbulence in the flow field was delineated in terms of the vortex structure, velocity profile, turbulent intensity, integral scale, and Taylor microscale. To avoid aliasing and to ensure reliability, 10^6 data points at

each measurement location were sampled at 80 kHz and low-passed at 30 kHz. The flow characteristics deduced were correlated with the heat transfer behaviour. According to Tennekes et al. [24], when the mean flow properties do not change significantly with time, the flow maybe assumed to be in a quasi-steady state. In this study, neither the mean flow nor the heat transfer properties changed noticeably with respect to time after the initial warming-up phase and hence, we invoked the steady-state assumption.

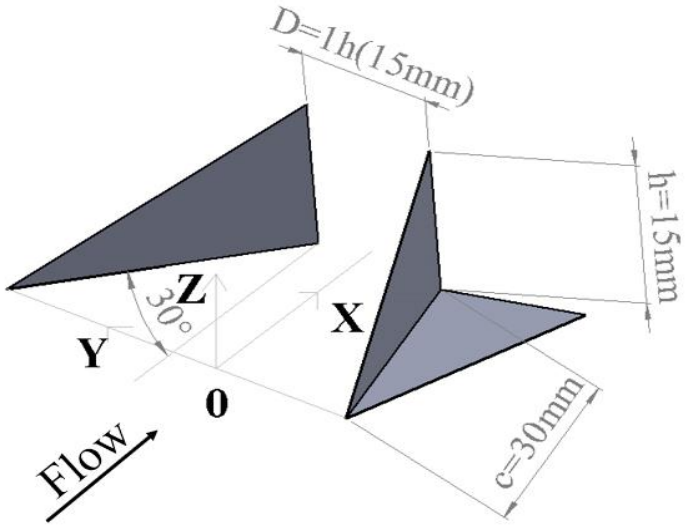

Figure 2.1. The winglet pair with chord length, c = 30 mm, height, h = 15 mm, attack angle, $\alpha = 30°$, separation, $D = h$.

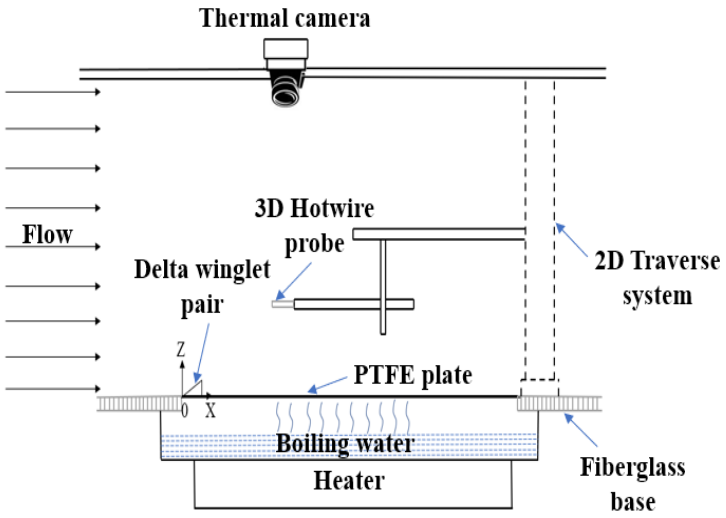

Figure 2.2. The experimental setup inside a wind tunnel. The bowl of water underneath the *PTFE* plate was boiling over the course of the experiment.

2.3 Data Analysis

The total heat conducted from the bottom to the top surface of the *PTFE* plate,

$$\dot{Q}_{Total} = \frac{k_{PTFE} \cdot A(T_{Bottom} - T_{Top})}{t_{PTFE}} \quad (1)$$

where *PTFE* plate conductivity, k_{PTFE}, was 0.25 $Wm^{-1}K^{-1}$ [22], the local heat transfer area, *A*, was 20 mm^2, the thickness of the *PTFE* plate, t_{PTFE}, was 3 mm, the bottom surface temperature, T_{Bottom}, was fixed at 373 K by the condensing steam, and the top surface temperature, T_{Top}, was measured by the thermal camera. With negligible horizontal conduction to the base of the wind tunnel, the heat conducted through the *PTFE* plate to the top surface either radiated to the surroundings or was convected by the incoming free stream. The heat that radiated to the surroundings was determined according to the Stefan-Boltzmann law,

$$\dot{Q}_{radiation} = \varepsilon \sigma A(T_{Top}^4 - T_{Wall}^4) \quad (2)$$

where the emissivity, ε, was 0.92 [23], the Stefan-Boltzmann constant, σ, was 5.67×10^{-8} [25] $Wm^{-2}K^{-4}$, and the wall temperature T_{Wall} was approximately 295 K. The convective heat transfer rate was deduced by subtracting the heat radiated to the surrounding from the total heat transfer rate.

$$\dot{Q}_{convection} = \dot{Q}_{Total} - \dot{Q}_{radiation} \tag{3}$$

The convective heat transfer coefficient,

$$H_{convection} = \frac{\dot{Q}_{convection}}{A(T_{Top} - T_{Air})} \tag{4}$$

The surrounding air temperature, T_{Air}, remained around 295 K during the experiment. The corresponding Nusselt number,

$$Nu = \frac{H_{convection} h}{k_{Air}} \tag{5}$$

The height of the winglet (h =15 mm) was taken as the characteristic length and the thermal conductivity of air, k_{air}, was 0.0262 $Wm^{-1}K^{-1}$ [22]. As we were interested in the heat transfer enhancement, we normalized the Nusselt number with the reference Nusselt number without the winglet pair, that is,

$$\frac{Nu}{Nu_0} = \frac{H_{convection}}{H_{convection.o}} \tag{6}$$

The reference convective heat transfer coefficient, $H_{convection.0}$, corresponded to the case without the winglet pair.

We calculated the time-averaged velocities according to,

$$\bar{U} = \frac{1}{N}\sum_{i=1}^{N} U_i \; ; \; \bar{V} = \frac{1}{N}\sum_{i=1}^{N} V_i ; \; \bar{W} = \frac{1}{N}\sum_{i=1}^{N} W_i \tag{7}$$

where N=10^6 data points. Here, U_i, V_i, and W_i signify the streamwise, widthwise and vertical instantaneous velocities, respectively [26].

We obtained the instantaneous fluctuating velocities by subtracting the time-averaged velocity from the instantaneous velocity, i.e., $u_i = U_i - \bar{U}, v_i = V_i - \bar{V}, w_i = W_i - \bar{W}$. The streamwise root-mean-square fluctuating velocity was deduced accordingly,

$$u_{rms} = \sqrt{\sum_{i=1}^{N} \frac{{u_i}^2}{N-1}} \tag{8}$$

Dividing this with the freestream velocity, U_∞, gave the non-dimensional local turbulent intensity [27],

$$Tu = \frac{u_{rms}}{U_\infty} \tag{9}$$

The integral scale signifies the energy-containing large eddies [28]. In this study, we estimated the integral time scale from the autocorrelation factor,

$$\rho(\tau) = \frac{\overline{u(t)u(t+\tau)}}{\overline{u^2(t)}} \tag{10}$$

With discrete signals, we realized this by invoking,

$$\rho(n\Delta t) = \frac{\frac{1}{N-n}\sum_{i=1}^{N-n}(u_i u_{i+n})}{\frac{1}{N}\sum_{i=1}^{N} u_i^2} \tag{11}$$

The integral time scale can be determined by integrating the autocorrelation factor,

$$\tau_\wedge = \int_0^\infty \rho(\tau) d\tau \tag{12}$$

We approximated this from the discrete signals as

$$\tau_\wedge = \sum_{i=1}^{N_K - 1} \rho(i\Delta t)\Delta t \tag{13}$$

N_K corresponded to the point where the autocorrelation first changed from positive to negative.

Multiplying the integral time scale with the time-averaged freestream velocity in *X*-direction, $\bar{U}$, gave the streamwise integral length scale,

$$\wedge = \bar{U}\tau_{\wedge} \tag{14}$$

In other words, we invoked the Taylor frozen hypothesis [28], assuming the relatively fast convection of the eddies across the hot-wire sensor as though they were frozen. At the studied measurement locations, the relative turbulence intensity, *Tu*, was largely less than 10% and thus, the Taylor frozen hypothesis was reasonably sound.

We also applied Taylor frozen hypothesis for deducing the streamwise Taylor microscale [28],

$$\lambda = \bar{U}\tau_{\lambda} \tag{15}$$

The Taylor time scale can be expressed as

$$\tau_{\lambda} = \sqrt{\frac{\overline{2u_i^2}}{(\frac{du_i}{dt})^2}} \tag{16}$$

For discrete data, we approximated this as

$$\tau_{\lambda} = \sqrt{\frac{\frac{1}{N}\sum_{i=1}^{N} 2u_i^2}{\frac{1}{N-1}\sum_{i=1}^{N-1}(\frac{u_{i+1}-u_i}{\Delta t})^2}} \tag{17}$$

We computed the vorticity of the longitudinal vortex based on

$$\omega = \frac{\partial \bar{W}}{\partial y} - \frac{\partial \bar{V}}{\partial z} \tag{18}$$

Multiplying this with the height of the winglet and dividing it with the freestream velocity, U_{∞}, gave the non-dimensional vorticity.

$$\Omega = \frac{\omega h}{U_{\infty}} \tag{19}$$

We determined the total uncertainty from bias uncertainty (B) and precision uncertainty (P) following Ref [29]. In this study, we based the bias certainty on the

calibration process, and the precision uncertainty on repeated measurements. The details of the uncertainty analysis are in the appendix.

Wu et al. [10] studied the impact of total turbulence fluctuation, velocity towards the heated surface, and near-surface streamwise velocity on heat transfer enhancement using delta winglets. According to their study, the total turbulence fluctuation was the largest contributor to heat transfer enhancement, followed by velocity towards the heated surface. The near-surface streamwise velocity had significantly smaller impact. We performed similar analysis in this study. We examined cross-stream vorticity, Ω, stream-wise time-averaged velocity, $\overline{U}/U_\infty$, vertical averaged, $\overline{W}/U_\infty$, stream-wise root-mean-square turbulence intensity, u_{rms}/U_∞, span-wise turbulence intensity, v_{rms}/U_∞, height-wise turbulence intensity, w_{rms}/U_∞, streamwise integral scale, Λ/h, and streamwise Taylor microscale, λ/h, on the heat transfer enhancement, Nu/Nu_0, using multiple linear regression analysis. To find the weight of impact, the standardised regression coefficients (β_j^{std}) were used [30],

$$\beta_j^{std} = \beta_j \frac{std_j}{std_y} \tag{20}$$

Here, β_j^{std} represents the standardized regression coefficient, denoting the impact of the individual studied flow parameters on the dependent variable (Nu/Nu_0), β_j and std_j are the regression coefficient and standard deviation of each of the studied individual parameter and std_y is the standard deviation of the dependent variable (Nu/Nu_0).

2.4 Results and Discussions

We focused on the effect of transverse distance between the trailing edges of the winglet pair on the augmentation of forced convection over the heated *PTFE* plate. As such, we normalized the local Nusselt number with the underlying reference Nusselt number without the delta winglets. We determined the various correlations at 10*h* downstream of the winglet pair where the flow was quasi-steady and representative of the average conditions over the entire plate.

2.4.1. Heat Transfer

Figure 2.3 shows the distribution of the normalized Nusselt number, Nu/Nu_0, on the inner portion, away from the boundary outside of which the bottom surface was not exposed to the condensing steam, of the *PTFE* plate. The uncertainty of Nu/Nu_0 was around 0.06. The dark triangles denote the winglets. The region in the immediate proximity of these winglets gave the highest Nu/Nu_0 primarily mostly because the aluminium winglets acted like heat fins. The intense vortical flows around the winglets resulted in more than 80% enhancement in Nusselt number, with Nu/Nu_0 = 1.8 contour up to X=3h downstream, for all studied cases (D=0, 1h, 2h, and 3h). Outside of this, a high Nu/Nu_0 = 1.3 region is seen up to X/h=7 (Y/h=1.5 to -1.5) for both D=0 and D=1h cases. This Nu/Nu_0 region of 1.3 is extended all the way downstream to X/h=11 for the D=3h case. More importantly, this high Nu/Nu_0 contour of 1.3 extended up to X/h=15 (Y/h= 0 to 1.5) when D=2h. Further, it is noticed that the D=2h case shows a consistent Nu/Nu_0 = 1.2 contour up to X/h of 19, which is not found in the other three cases. The general diminishing enhancement with distance downstream, due to decaying turbulence and vortex intensity, becomes more visible beyond X=14h. It is also noted that for the

most sparsely spaced winglet pair with D=3h, the narrow strip between the two winglets (Y=±0.75h) a normalized Nusselt number of no more than 1.05 is observed. In fact, there is a narrow region where Nu/Nu_0 is less than one. This hints that there is a lack of positive heat transfer enhancing interaction between the flow structures generated by the two winglets. That is, the winglet pair acted largely as two isolated winglets with a narrow region of diminishing heat transfer possibly because of the merging of near-surface hot air brought about by the counter-rotating vortex streets generated by the sparsely separated winglets.

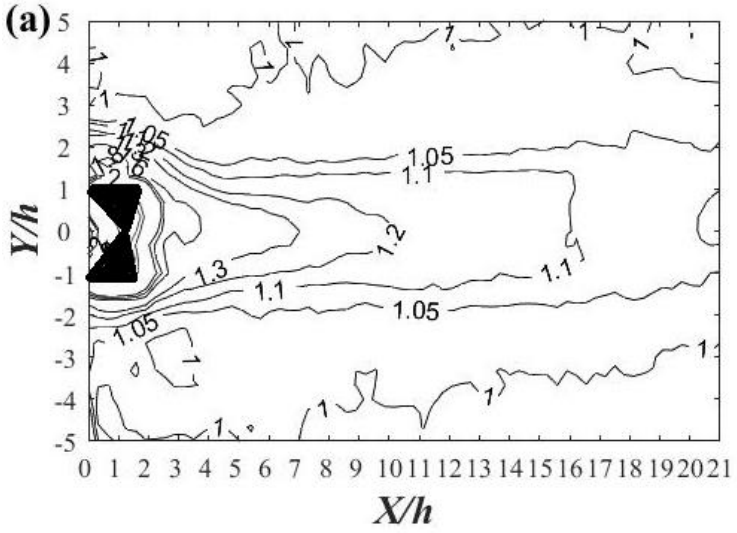

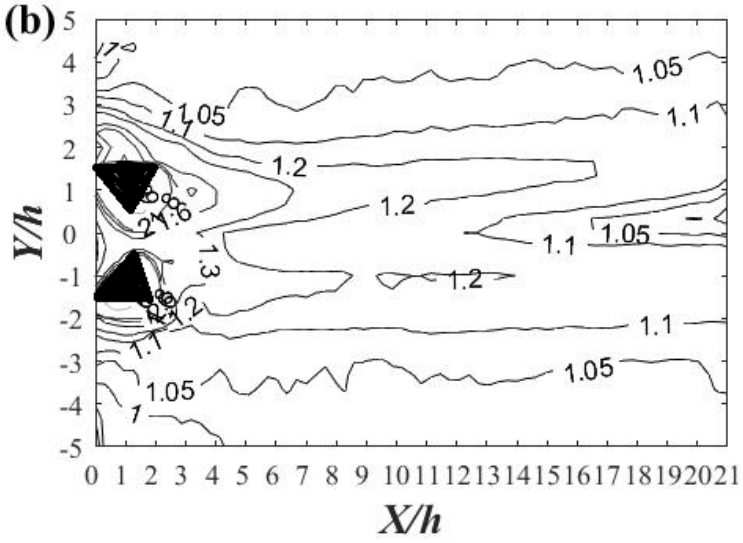
(b)
Y/h
X/h
1.05
1.1
1.2
1.3

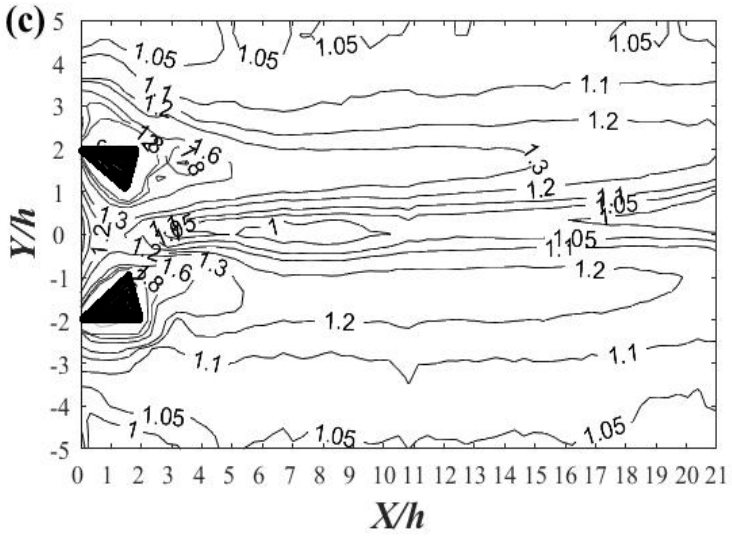
(c)
Y/h
X/h
1.05
1.1
1.2
1.3
1.6
1.8

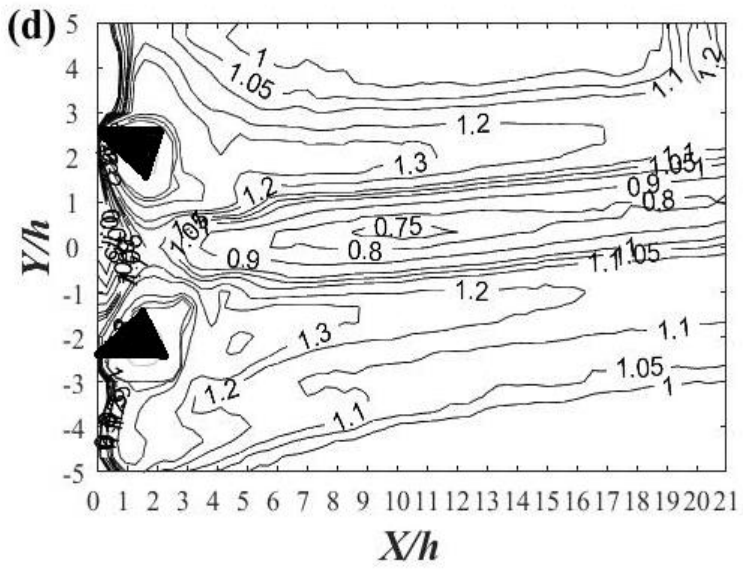

Figure 2.3. The normalized Nusselt number, Nu/Nu_0, distribution for the winglet pair with (a) D= 0 (b) D=1h (c) D=2h and (d) D=3h.

Figure 2.4 depicts the effect of transverse distance between the trailing edges of the winglet pair on the cross-sectional Nu/Nu_0 profile at various downstream distances. It is noted that at X=5h, the 2h-spaced winglet pair produced a peak Nu/Nu_0 of nearly 2.1 at Y=-2.0h, significantly higher than those of 0-, 1h-, and 3h-spaced winglet pair which were around 1.0, 1.30, and 1.45, respectively at the same location. This peak Nu/Nu_0 observed at Y/h of -2.0 obtained at D=2h tends to decrease farther downstream, specifically, $Nu/Nu_0 \approx$ 2.10, 1.40 and 1.37 at X/h = 5, 10, & 15, respectively at the same cross-stream location. The 2h spaced winglet pair provided the highest Nu/Nu_0 of approximately 1.40 at X=10h and Y=-2.0h. This value is much larger than those associated with 0-, 1h-, and 3h-spaced winglet pairs, whose values are around 1.05, 1.20, and 1.30, respectively. It is also noted that at Y/h=0, and X/h=10, a high Nu/Nu_0 of 1.20 is observed for D=0; at the same location the Nu/Nu_0 for 1h-, 2h-, and 3h-spaced winglets

are significantly lower, around 1.17, 1.0, and 0.75, respectively. This hints that there is a lack of fresh cooler air from the freestream moving into and approaching the hot surface. The location of the low (less than one) Nu/Nu_0 value has been found to be associated with the outflow region [31], indicating the warmer near-surface air from the neighboring near-surface was brought into this region before it is swept away from the hot surface, reducing the local heat transfer rate. We see that even far downstream at X=15h, the 2h-spaced winglet pair continued to significantly enhance the cooling of the hot plate, with Nu/Nu_0 around 1.30 at Y/h=-2.0. At that same location, Nu/Nu_0 corresponding to the 0-, 1h-, and 3h-spaced winglet pairs are approximately 1.0, 1.17, and 1.20, respectively.

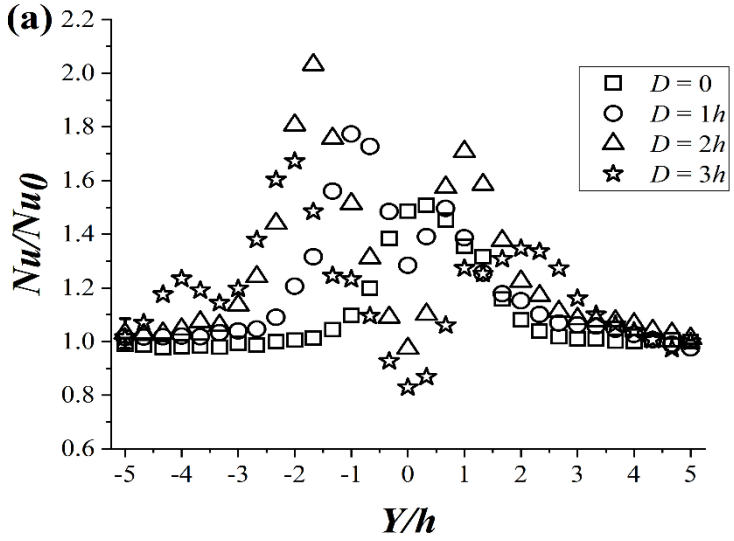

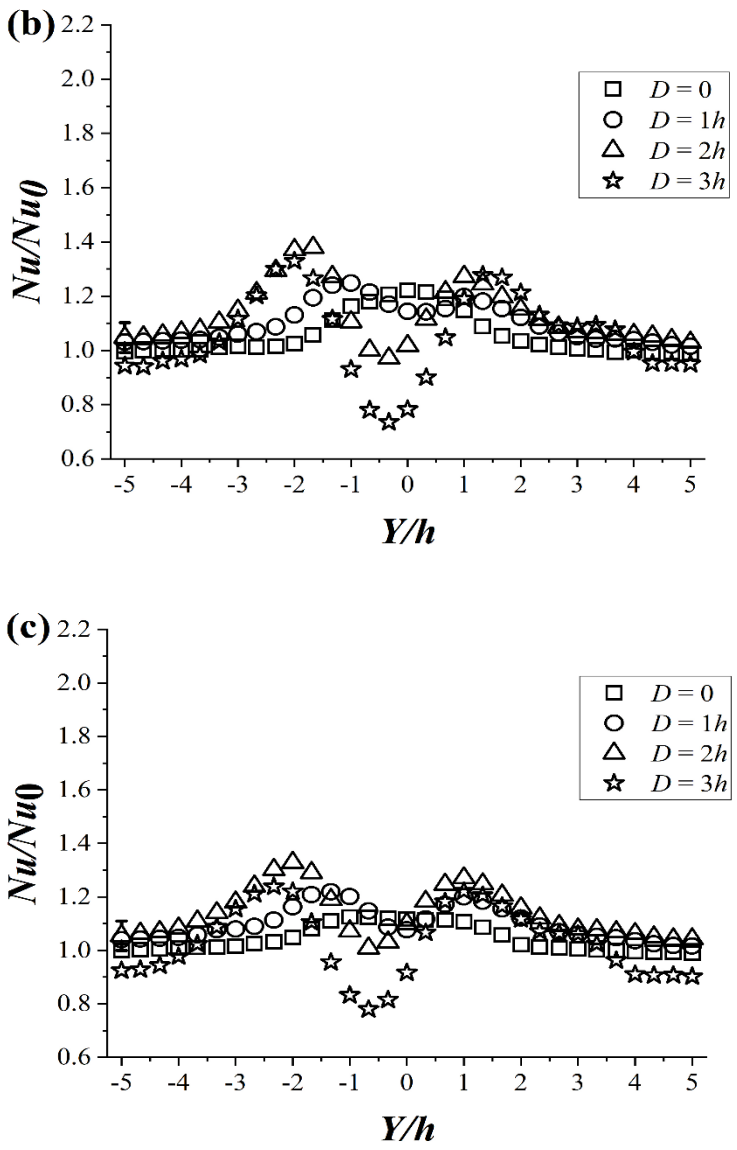

Figure 2.4. The effect of transverse distance between the trailing edges of the winglet pair (D=0, D=1h, D=2h & D=3h) on the cross-sectional Nu/Nu_0 profile at (a) X=5h, (b) X=10h and (c) X=15h downstream.

The average, rather than localized Nu/Nu_0, $Nu_{avg}/Nu_{0,\,avg}$, is of importance in engineering applications, such as the cooling of a solar panel. Figure 2.5 compares the centerline, along Y=0, Nusselt number, Nu/Nu_0, with that averaged over Y= ±3h, $Nu_{avg}/Nu_{0,\,avg}$. The Nu/Nu_0 of less than one stretch for D=3h case at Y=0 observed in

Figure 2.3 is clearly seen in Figure 2.5(a); this heat transfer reduction is not seen in the other three (*D*=*0*, 1*h* and 2*h*) cases. Nonetheless, values of $Nu_{avg}/Nu_{0,\,avg}$ for all cases, including the *D*=3*h* case as shown in Figure 2.5(b) are above one. This indicates that the use of winglets over the tested range of conditions always improve the overall heat transfer rate. More importantly, the *D*=2*h* case is consistently superior over the entire studied plate area, this is followed by the *D*=1*h* case. To understand the underlying physics, we take a close look at the flow characteristics in the next section.

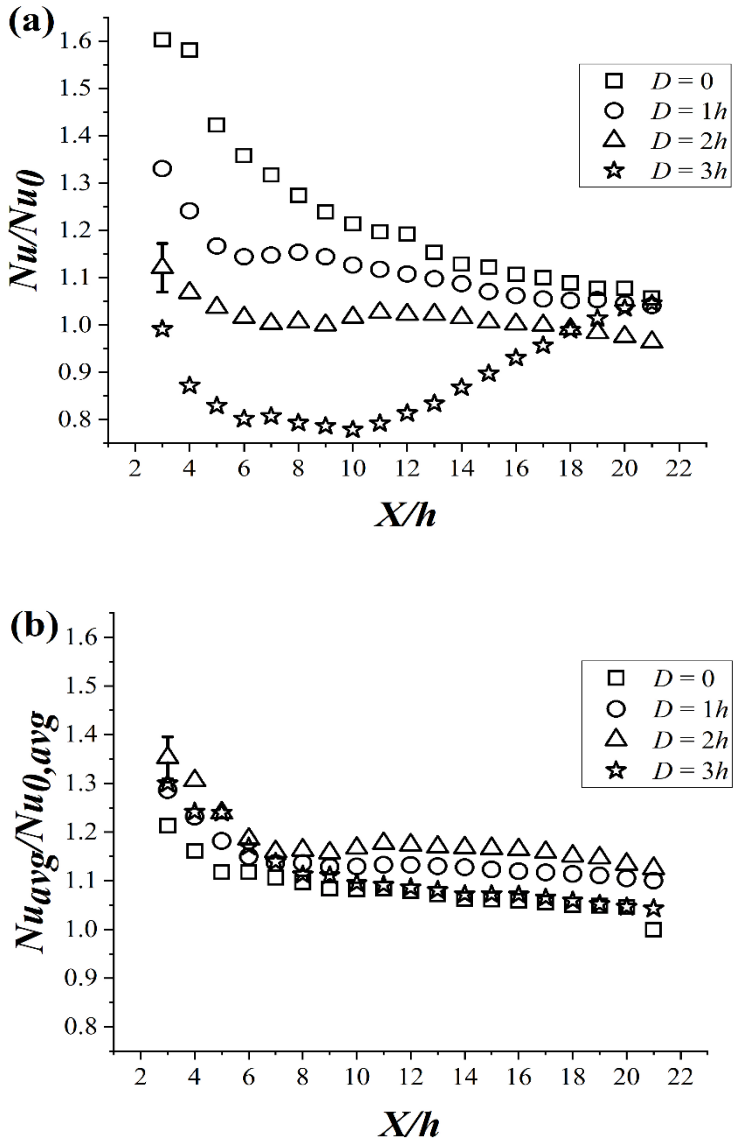

Figure 2.5. Normalized Nusselt number distribution downstream of the winglets (a) local value, Nu/Nu_0, along the center of the wing pair, Y=0, and (b) value averaged over Y= ±3h, $Nu_{avg}/Nu_{0,\,avg}$.

2.4.2. Flow Characteristics

The winglet pair was taped onto the *PTFE* plate with origin O defined as the midpoint of between the leading edges of the pair of winglets; see Figures 2.1 and 2.2. The vortical flow reached a slowly-decaying, quasi-steady condition between 5h and 10h downstream of the winglet pair. Therefore, the turbulent flow characteristics generated by the delta-winglet pair over the unheated *PTFE* plate were measured at 10h (150mm) downstream of the leading edge of the winglet pair for three spacing conditions of D=0, 1h and 2h between the trailing edges. We used a 3D hot wire probe (type 55P95) and a constant temperature anemometer to measure the wind velocity. We then decomposed the measured velocity into the three orthogonal components and delineated these velocities in terms of vortex structure, velocity profile, turbulence intensity, integral scale, and Taylor microscale [26]. We depict the pair of winglets, when viewed from downstream to upstream, as triangles with dotted lines in the upcoming figures.

2.4.2.1. Vortex Structure

The cross-stream vorticity contours at 10h downstream are shown in Figure 2.6. The uncertainty in vorticity (Ω) was estimated to be 0.004. Decreasing the transversal spacing from D=2h to D=0 resulted in a decrease in non-dimensional X-direction vorticity from 0.4 to 0.1. This is similar to what was observed by Yang et al [32] and Sun et al [33]. Among others, Wu [34] noted that the swirling vortical motions promoted downward flow towards the hot surface, bringing in cooler air from the freestream to

carry away the heat from the surface. Figure 2.6 shows two main vortices, one rotating clockwise and the other anti-clockwise. These counter-rotating vortices induced an upward flow in the common region between the two vortices for the D=1h and D=2h cases. The plate surface areas corresponding to the highest vorticity regions at the core of the vortices, at the same Y/h values, coincided roughly with the peak Nu/Nu_0 regions in Figure 2.4. This is because the vortex-induced tangential sweeping of air across the hot surface is most intense at these near-surface regions. Furthermore, these vortices tended to move closer to the surface as the transverse distance was increased from D=1h to D=2h. Consequently, the vorticity at the vortex core increased from 0.3 to 0.4 and hence, the corresponding enhancement in heat transfer.

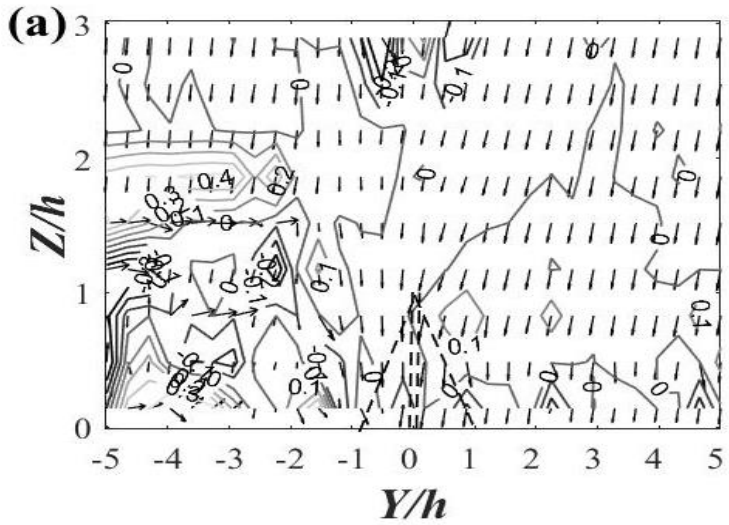

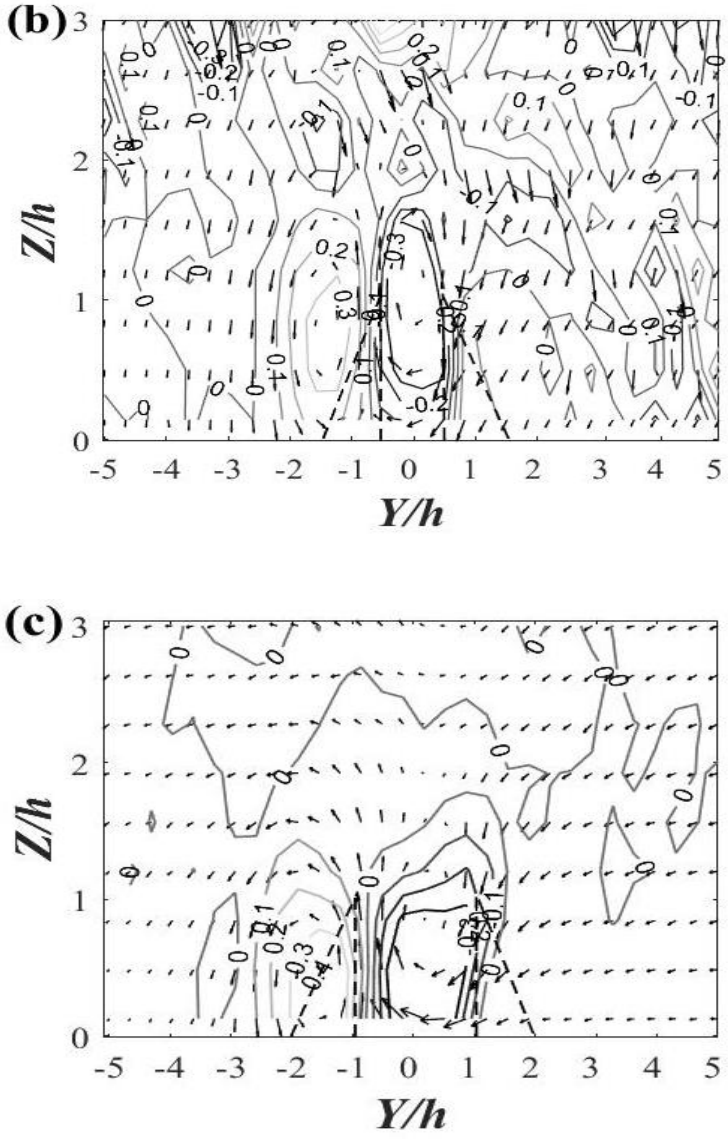

Figure 2.6. Normalized cross-stream vorticity contours for (a) *D*=0 (b) *D*=1*h* and (c) *D*=2*h*, at 10*h* downstream from the leading edge of the winglets.

2.4.2.2. Velocity Profile

The air moving along the plate in the stream-wise direction is known to affect the heat transfer rate. Figure 2.7 shows the time-averaged stream-wise velocity contours normalized by U_∞ along with the velocity vectors at *YZ* plane. The uncertainty of the mean stream-wise velocity was approximately 0.28 m/s and the uncertainty in $\bar{U}/U_\infty$ was

around 0.040. With an increase in transversal spacing, *D*, from 0 to 2*h*, the boundary layer became thinner. We can clearly see that the $0.9U_{\infty}$ contour approaches the plate with increasing *D* from 0 to 2*h*. The cooling becomes more effective as faster moving fluid moves nearer to the hot surface. In other words, the thinning of the boundary layer contributed to the increasing Nu/Nu_0 as *D* increased from 0 to 2*h*.

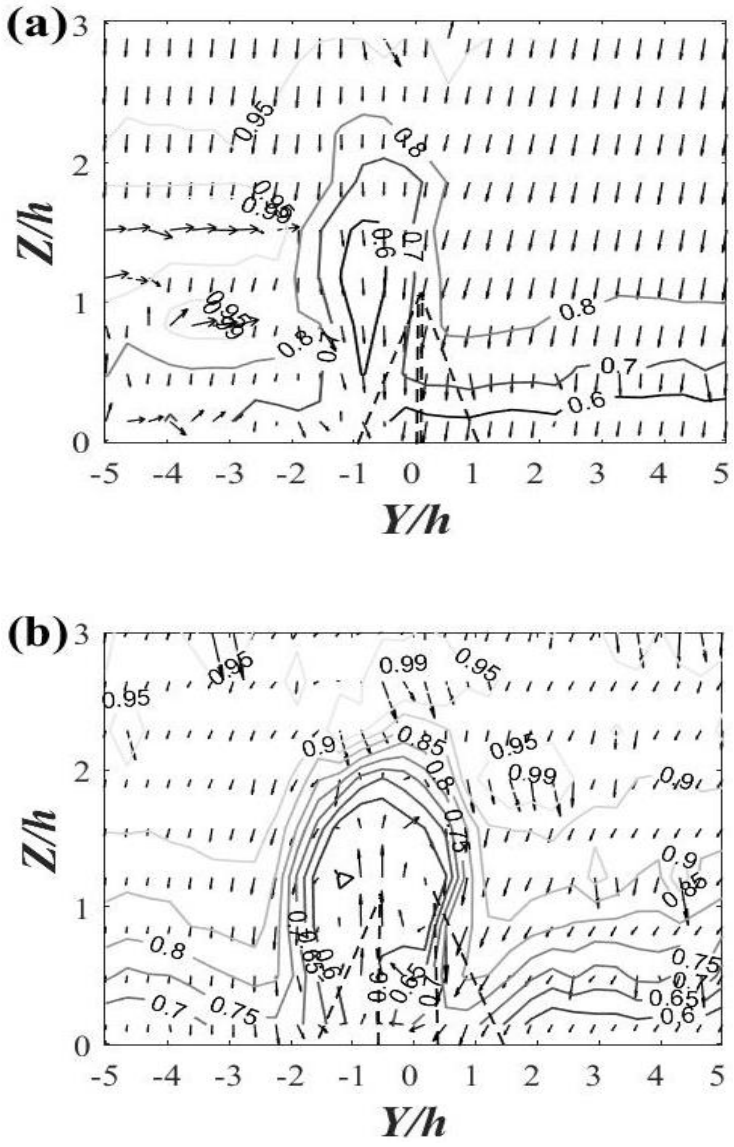

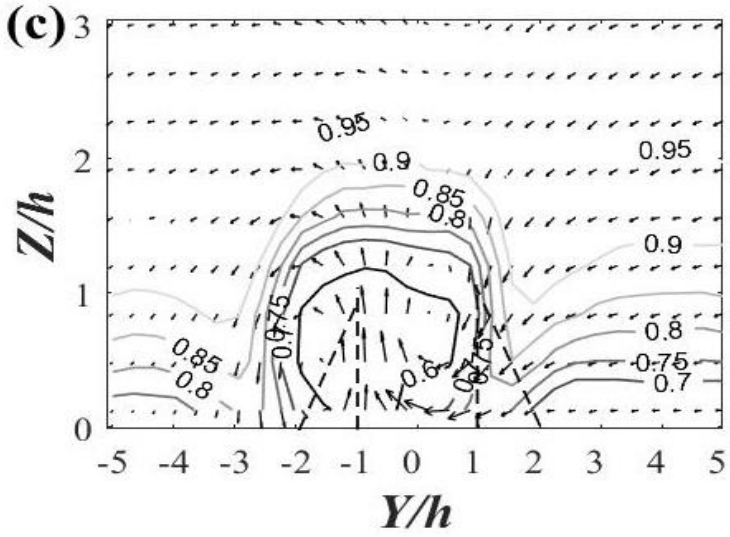

Figure 2.7. Normalized stream-wise time-averaged velocity ($\bar{U}/U_\infty$) contours and velocity vectors at *YZ* plane for (a) *D*=0 (b) *D*=1*h* and (c) *D*=2*h*, at 10*h* downstream from the leading edge of the winglets.

The downward wind velocity towards the hot surface also plays a significant role in heat convection [10]. The normalized vertical velocity, $\bar{W}/U_\infty$, measured at *Z* = 0.33*h*, and 10*h* downstream of the winglet pair is plotted in Figure 2.8. The uncertainty in $\bar{W}$ was approximately 0.021 m/s, leading to an uncertainty in $\bar{W}/U_\infty$ of around 0.003. For the winglets with their trailing edges in contact with each other, *D*=0, a substantial downwash velocity of -0.105 is observed at *Y/h*= 0, which roughly coincided with the peak *Nu/Nu₀* in Figure 2.4. In general, the locations of the lowest and largest $\bar{W}/U_\infty$ roughly coincided with the inflow and outflow regions in Figure 2.7. For example, the 2*h*-spaced winglet pair recorded a most negative $\bar{W}/U_\infty$ of -0.085 in the inflow region and a most positive $\bar{W}/U_\infty$ of 0.105 in the outflow region. The associated most negative and most positive $\bar{W}/U_\infty$ for the 1*h*-spaced winglet pair are around -0.06 and 0.09, respectively. In other words, increasing the transverse distance from *D*=1*h* to 2*h* resulted

in more cold air flow towards the hot plate at the more negative $\bar{W}/U_\infty$ region and more hot air scooped away from the plate at the more positive $\bar{W}/U_\infty$ region. It appears that a significant inflow followed by an equally significant outflow furnishes the most effective "heat scooper"; this is a probable reason why D=2h case is superior to D=1h and 0 cases.

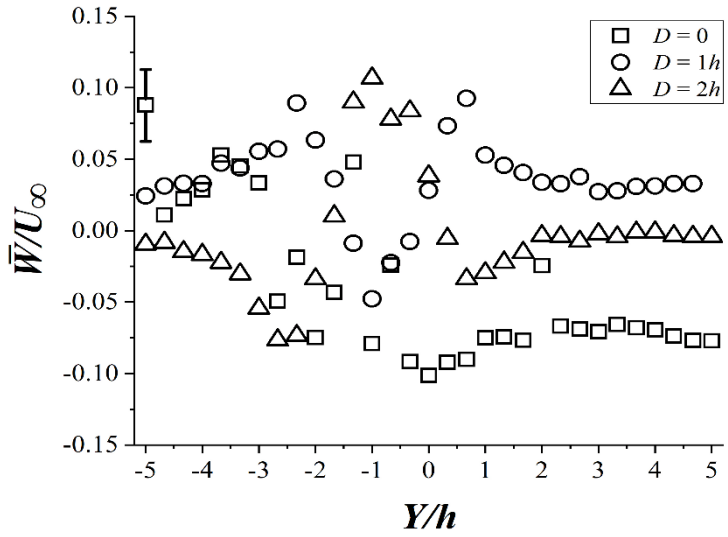

Figure 2.8. Normalized vertical velocity, $\bar{W}/U_\infty$, measured at Z = 0.33h above the plate, at X=10h downstream of the winglet pair.

2.4.2.3. Turbulent Intensity

The flow turbulent intensity also plays a significant role in convective heat transfer [10]. Figure 2.9 depicts the turbulence intensity (Tu is the local turbulence root-mean-square fluctuation u_{rms}, normalized by the freestream time-averaged velocity, U_∞) contours at 10h (150 mm) downstream the winglet pair. The uncertainty of freestream turbulent intensity was estimated to be around 0.004. With the heat transfer bottleneck imposed by the boundary layer where the fluid slows down to zero at the solid surface, the near-surface turbulence is most critical in mitigating this heat transmission bottleneck.

It is clear from Figures 2.9 that the near-surface turbulence intensity increases with increasing *D* from zero to 1*h*, to 2*h*. This is consistent with the increasing Nu/Nu_0 results.

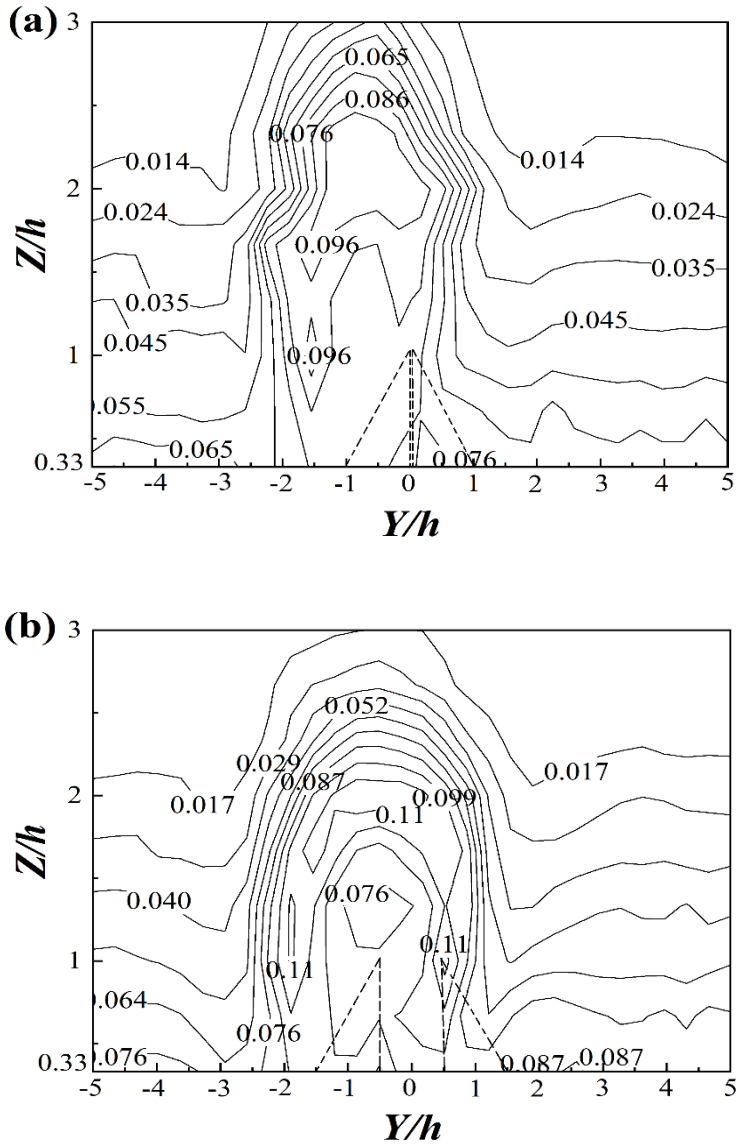

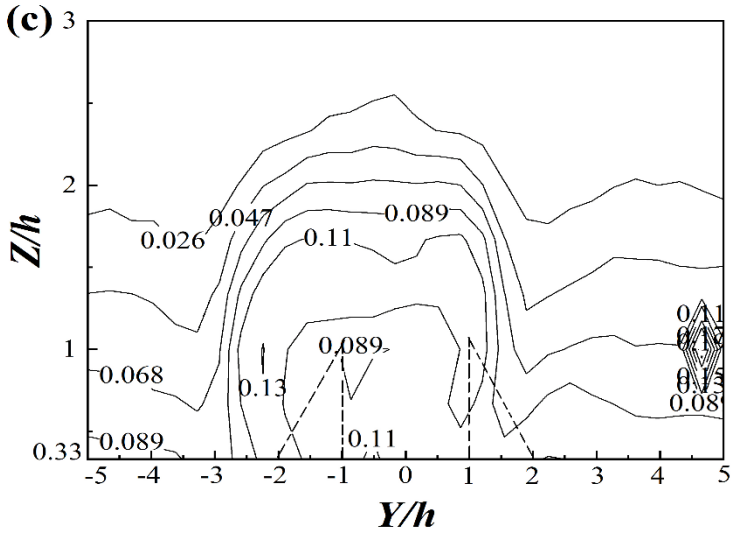

Figure 2.9. Normalized stream-wise turbulent intensity (u_{rms}/U_{∞}) contours in the *YZ* plane for (a) D=0 (b) D=1*h* and (c) D=2*h*, at 10*h* downstream from the leading edge of the winglets.

2.4.2.4. Integral Scale

The integral scale is of interest because most of the turbulent kinetic energy is contained in the eddying motions described by it [28]. The steam-wise contours of the integral scale (Λ) normalized by winglet height (h =15 mm) in the *YZ* plane is shown in Figure 2.10. Note that outside of the wake and boundary layer regions, the flow turbulence is relatively weak and hence, the corresponding integral scale is not well defined. Within the well-defined turbulent region of interest, the uncertainty of integral length normalized by winglet height scale was estimated to be 0.04. No clear trend of systematic variation stream-wise integral scale value with respect to changing *D* is discernible from the figure. We will examine the role Λ on Nu/Nu_0 based on multiple linear regression analysis in a latter section.

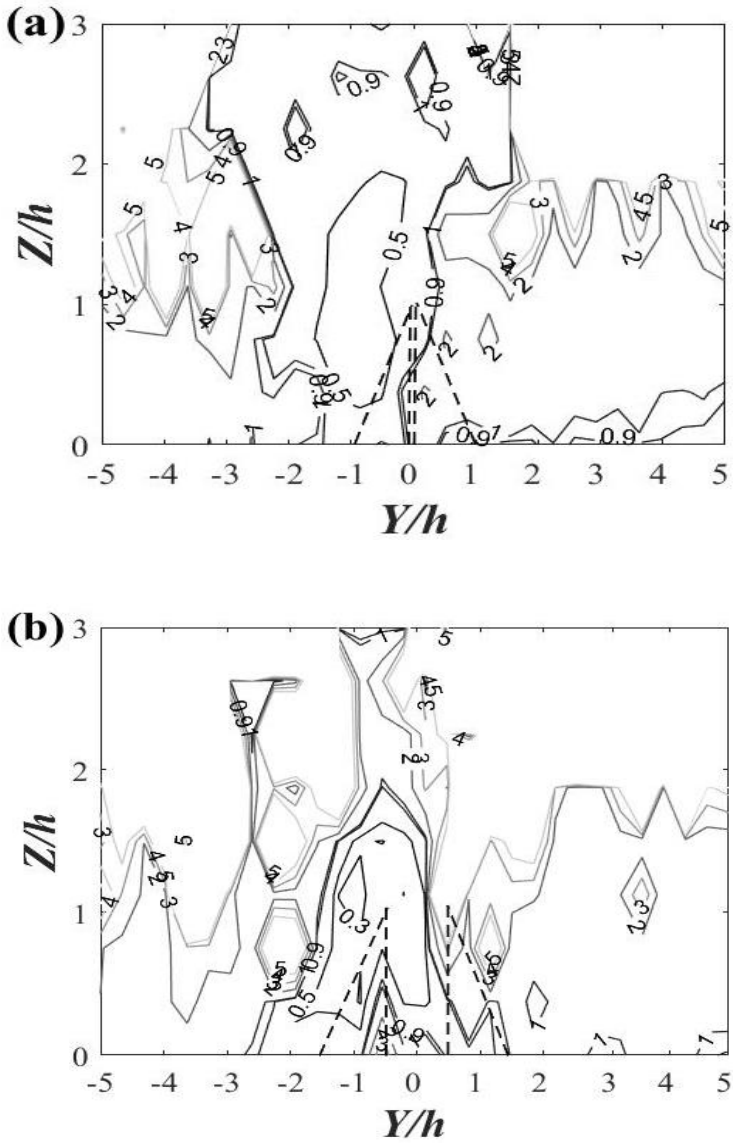
(a)
Z/h
Y/h
(b)
Z/h
Y/h

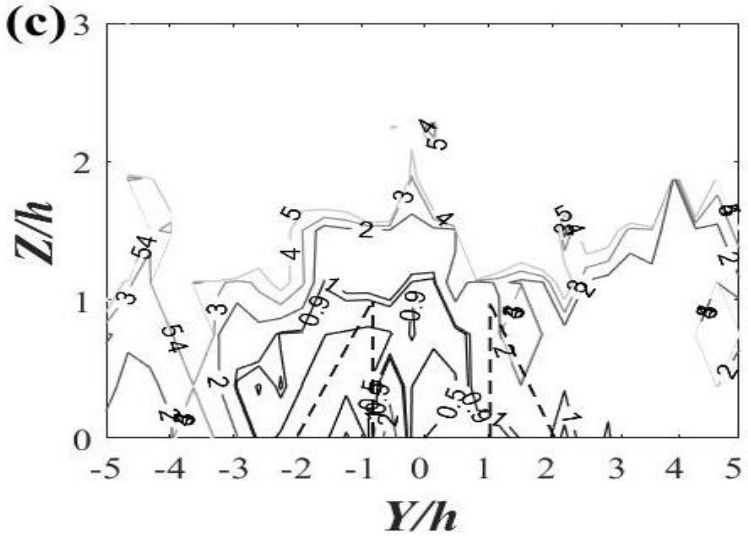

Figure 2.10. Normalized stream-wise integral scale, Λ/h, contours in *YZ* plane for (a) D=0 (b) D=1h and (c) D=2h, at 10h downstream.

2.4.2.5. Taylor Microscale

The Taylor microscale represents the dissipative end of the turbulence energy cascade and thus is also of interest in heat convection [28]. The contour view of the stream-wise Taylor microscale normalized by the winglet height (15 mm) is shown in Figure 2.11. The uncertainty of the normalized Taylor microscale was estimated to be 0.004. From the figure, it is evident that the low Taylor microscale regions roughly coincide with the maximum turbulent intensity zones in Figure 2.9 and the high Nu/Nu_0 areas in Figure 2.4. Similar to the integral scale results, it is difficult to quantify the influence of D on Taylor microscale, and its subsequent effect on Nu/Nu_0, based on the contour plots. Therefore, we will resort to the multiple linear regression analysis.

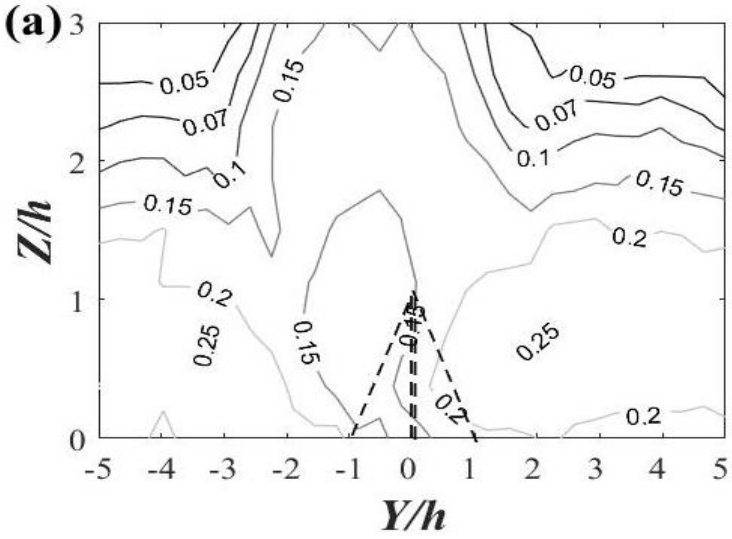
(a)
Z/h
Y/h
0.05
0.07
0.1
0.15
0.2
0.25

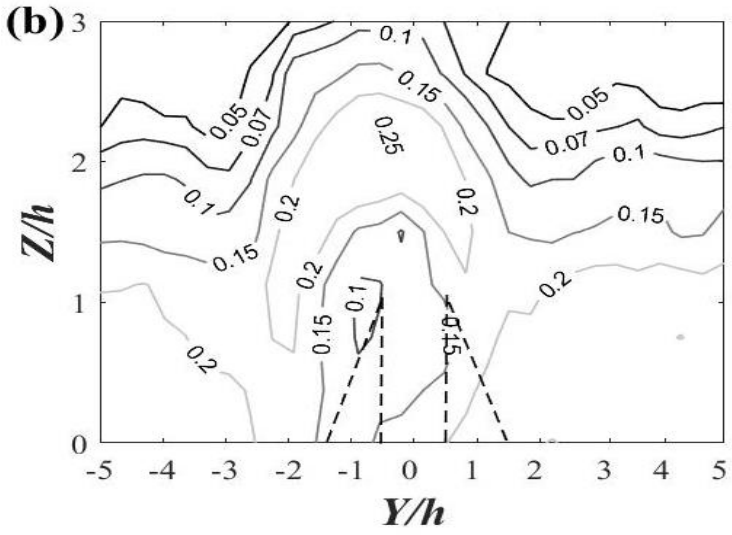
(b)
Z/h
Y/h
0.05
0.07
0.1
0.15
0.2
0.25

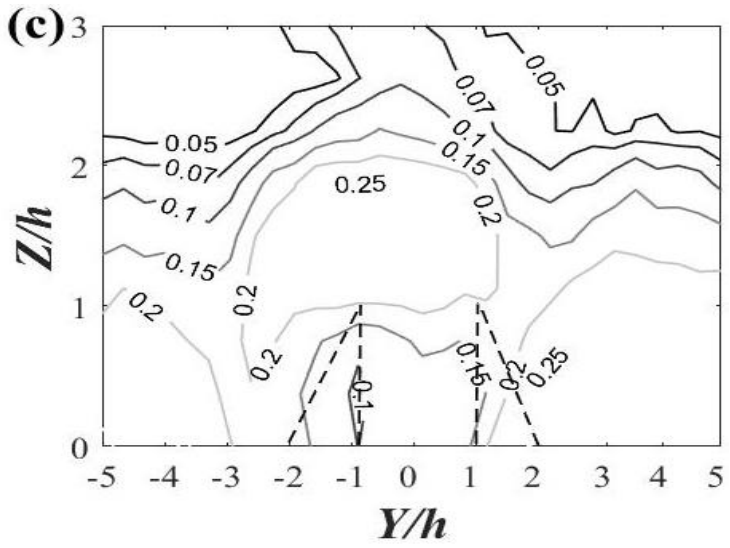

Figure 2.11. Normalized stream-wise Taylor microscale, λ/h, contours in *YZ* plane for (a) D=0 (b) D=1h and (c) D=2h, at 10h downstream.

2.4.3. Regression Analysis

Based on the heat transfer and flow characteristics described above, it can be inferred that the heat transfer augmentation is influenced by various flow mechanisms. The individual effects of the normalized vertical velocity, $\overline{W}/U_\infty$, the stream-wise velocity normalized by the time-averaged free-stream velocity, $\overline{U}/U_\infty$, and the local height-wise turbulent intensity normalized by time-averaged free-stream velocity, w_{rms}/U_∞, on the heat transfer enhancement (Nu/Nu_0) are of interest. To compare their respective significance, a regression analysis was performed by fitting the data at X=10h, spanning the cross-section defined by Y=±3h, and at Z=0.33h. The raw data of the regression analysis are plotted in Figure 2.12. The correlations between other studied flow parameters and Nu/Nu_0 appear similarly scattered and are not included in this manuscript. Amidst the scatter, we can still see that certain flow parameters correlate better with the heat transfer enhancement than others. The significant scatter is primarily

because every data point corresponds a condition where the values of the different flow parameters are unique to that data point. For example, when correlating Nu/Nu_0 with $\bar{W}/U_\infty$ in Figure 2.12(a) for D=1h case, the data points correspond to changes in w_{rms}/U_∞, $\bar{U}/U_\infty$, and others, in addition to variation in $\bar{W}/U_\infty$. As such, a multiple linear regression analysis is more appropriate.

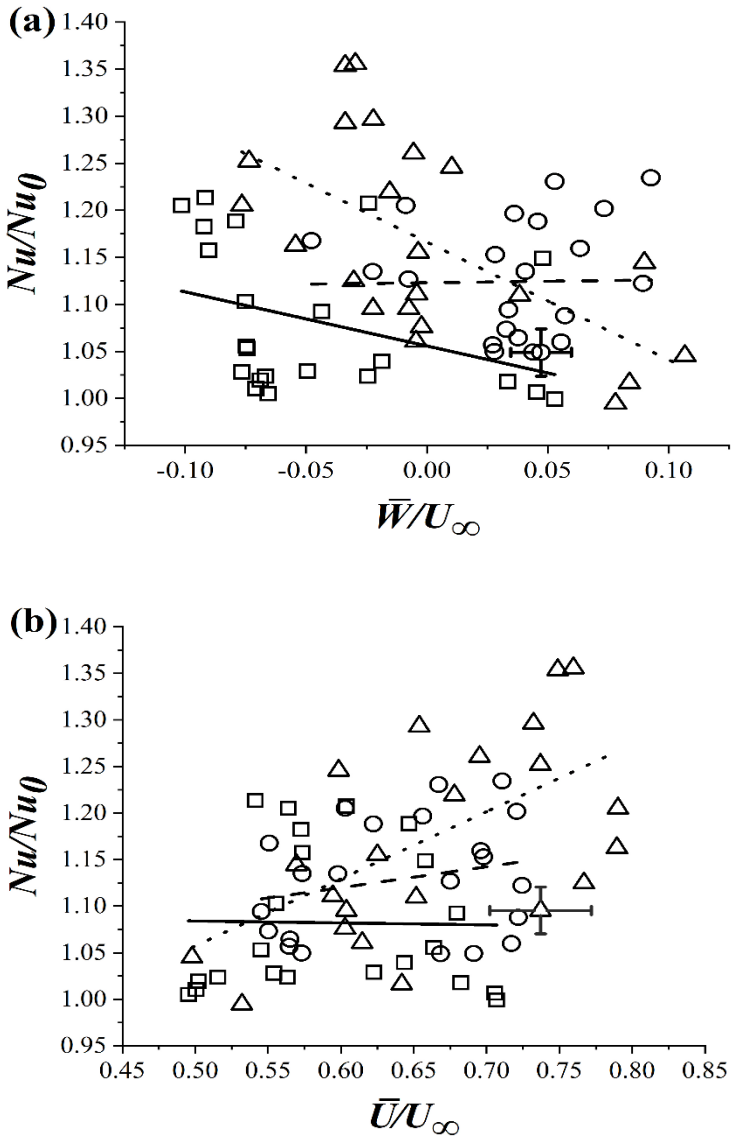

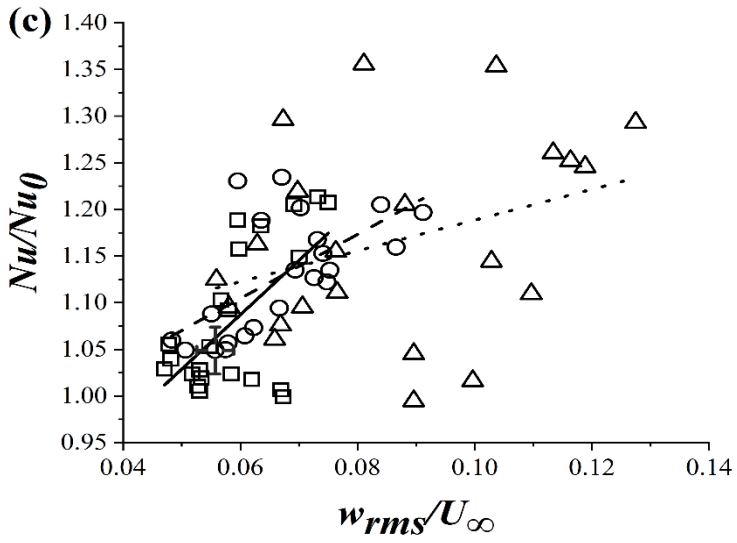

Figure 2.12. Correlating normalized (a) vertical velocity, $\overline{W}/U_\infty$, (b) stream-wise velocity, $\overline{U}/U_\infty$, and (c) local vertical turbulent intensity, w_{rms}/U_∞, with Nu/Nu_0 at X=10h, Y=±3h, and Z=0.33h. The solid, dashed, and dotted lines represent the linear fits for D=0, D=1h and D=2h cases, respectively. R-square values of $\overline{W}/U_\infty$ are 0.13, 0.00 and 0.36 for D=0, D=1h and D=2h cases, respectively. R-square values of $\overline{U}/U_\infty$ are 0.00, 0.06 and 0.58 for D=0, D=1h and D=2h cases, respectively. R-square values of w_{rms}/U_∞ are 0.38, 0.38 and 0.11 for D=0, D=1h and D=2h cases, respectively.

A multiple linear regression analysis was performed to delineate the relatively significance of dimensionless cross-stream vorticity, Ω, stream-wise time-averaged velocity, $\overline{U}/U_\infty$, vertical averaged, $\overline{W}/U_\infty$, stream-wise turbulence intensity, u_{rms}/U_∞, span-wise turbulence intensity, v_{rms}/U_∞, height-wise turbulence intensity, w_{rms}/U_∞, streamwise integral scale, Λ/h, and streamwise Taylor microscale, λ/h, with respect to the local heat transfer enhancement, Nu/Nu_0. The results are summarized in Table 2.2. Only the values corresponding to the data points closet to the plate at Z=0.33h were employed

in the analysis. This is because we expect the local flow characteristics to have the largest impact on heat convection from the hot plate.

Table 2.2. Multiple linear regression results.

Parameter	w_{rms}/U_∞	$\overline{U}/U_\infty$	$\overline{W}/U_\infty$	u_{rms}/U_∞	Ω	Λ/h	λ/h	v_{rms}/U_∞
β_j^{std}	0.657	0.497	0.416	0.370	-0.192	-0.099	0.064	0.015

The weight of each parameter on the heat transfer enhancement in Table 2.2 was determined by the absolute value of the standardised regression coefficient (β_j^{std}). It is clear that among the studied parameters, the vertical turbulent intensity, w_{rms}/U_∞, has the largest influence on the heat transfer enhancement. This indicates that the velocity fluctuation in the vertical direction is most effective in bringing the warmer fluid away from the hot plate and the cooler one onto the hot plate, resulting in significant cooling of the plate. The second most effective parameter is the stream-wise velocity, $\overline{U}/U_\infty$,which is closely followed by the velocity perpendicular to the plate, $\overline{W}/U_\infty$. In practise, we need a continuous flow of air over a heated surface such as a photovoltaic panel to keep it cool. Along the long span of a photovoltaic panel or an array of panels, the near-surface air will become warm and hence loses its cooling capability. Therefore, the into- and out-of-the-plate vertical flow comes to help. Downstream of the winglet pair, especially the pair that is separated by D=2h apart, the streets of organized vortices effectively realize this by swirling cooler air farther away in the freestream onto the hot surface while scooping away the warmer near-surface air into the freestream. Extending the span in the stream-wise direction is expected to reverse the order of $\overline{U}/U_\infty$ and $\overline{W}/U_\infty$ in Table 2.2, that is, lowering the value of β_j^{std} of $\overline{U}/U_\infty$ while increasing that associated with $\overline{W}/U_\infty$. The

stream-wise turbulence intensity, u_{rms}/U_∞, ranked fourth, with less than 60% of the weight of its vertical counterpart, w_{rms}/U_∞. This clearly illustrates the importance of mixing hot and cold fluid (vertically) across the boundary layer for effective heat transfer. The magnitude of the cross-stream vorticity, Ω, has a relatively small weight. More interestingly, it is negatively correlated with $\overline{U}/U_\infty$. Recall that we have utilized only the next-to-the-surface data points, and that vorticity is highest at the core of the organized vortices that are somewhat away from the plate. Around the edge of a vortex the vorticity is low. The near-surface regions marked by the two vertical edges of an organized vortex in this study corresponded to the inflow and outflow regions (Figure 2.4), and they, especially the inflow, correlated strongly with high Nu/Nu_0. This likely resulted in the negative correlation between near-surface vorticity and Nu/Nu_0. In other words, it is not the decrease in vorticity that improved the local heat convection, it is the associated inflow and outflow motions. As portrayed in Figures 2.10 and 2.11, the effects of Λ/h and λ/h are not obvious. The low values of β_j^{std} confirmed that this is indeed the case. Furthermore, the slightly negative value of β_j^{std} for Λ/h substantiates that an increase in integral length, which implies weaker turbulence, weakens $\overline{U}/U_\infty$. On the other hand, the small positive value of β_j^{std} for λ/h seems to convey that when an eddy is too small it loses its influence. The last-ranked parameter is the cross-stream turbulent fluctuation, v_{rms}/U_∞. It appears that the organized cross-stream motion induced by the organized vortices almost completely overshadowed the impact of w_{rms}/U_∞.

2.4. Conclusion

We experimentally investigated the role of the transverse distance between the trailing edges of a pair of winglets, D=0, D=1h, D=2h and D=3h, at Re_h=6300 on forced convection from a flat surface. The winglets of 30 mm chord length and 15 mm height were positioned with an attack angle 30° with respect to the wind. The heat transfer rate in terms of the normalized Nusselt number, Nu/Nu_0, was most significantly enhanced by the D=2h pair. This pair of optimally-spaced delta winglets consistently resulted in the most potent heat transfer augmentation in terms of maximum peak Nu/Nu_0 over an extended stretch of surface and highest average Nusselt number, $Nu_{avg}/Nu_{0,\,avg,}$ over the entire tested surface. Multiple linear regression analysis considering cross-stream vorticity, Ω, stream-wise time-averaged velocity, $\bar{U}/U_\infty$, vertical time-averaged velocity, $\bar{W}/U_\infty$, stream-wise turbulence intensity, u_{rms}/U_∞, span-wise turbulence intensity, v_{rms}/U_∞, height-wise turbulence intensity, w_{rms}/U_∞, streamwise integral scale, Λ/h, and streamwise Taylor microscale, λ/h, with respect to the normalized Nusselt number, Nu/Nu_0, was performed. The analysis demonstrated that turbulent fluctuation vertically into and out of the plate (boundary layer), as defined by $w_{rms}/U_{\infty,}$ has the largest influence on the heat transfer enhancement. The second most influential flow parameter is the stream-wise velocity, $\bar{U}/U_\infty$,which is responsible for moving the incoming air over the plate. Over the range of studied conditions, the velocity perpendicular to the plate, $\bar{W}/U_\infty$ that brings in freestream cool air into the hot plate has the third largest impact on the heat transfer rate. Ranking fourth is the stream-wise turbulence intensity, u_{rms}/U_∞, which is less than 60% as influential as its normal-to-the-plate counterpart w_{rms}/U_∞. The D=2h winglet pair

furnished the largest values of these most effectual flow parameters primarily via a pair of vibrant counter-rotating vortex streets that are closest to the plate.

Acknowledgement

This work was made possible by the Natural Sciences and Engineering Research Council of Canada and the Ontario Centers of Excellence.

References

[1] Rosenbloom, D., Meadowcroft, J. (2014). Harnessing the Sun: Reviewing the potential of solar photovoltaics in Canada. Renewable and Sustainable Energy Reviews, 40, 488–496.

[2] Vinoth Kanna, I., Pinky, D. (2020). Solar research–a review and recommendations for the most important supplier of energy for the earth with solar systems. International Journal of Ambient Energy, 41(8), 962–968.

[3] Teo, H. G., Lee, P. S., Hawlader, M. N. A. (2012). An active cooling system for photovoltaic modules. Applied Energy, 90 (1), 309-315.

[4] Rabie, R., Emam, M., Ookawara, S., Ahmed, M. (2019). Thermal management of concentrator photovoltaic systems using new configurations of phase change material heat sinks. Solar Energy, 183, 632–652.

[5] Bayrak, F., Oztop, H. F., Selimefendigil, F. (2020). Experimental study for the application of different cooling techniques in photovoltaic (PV) panels. Energy Conversion and Management, 212, 112789.

[6] Jakhar, S., Soni, M. S., Gakkhar, N. (2016). Historical and recent development of concentrating photovoltaic cooling technologies. Renewable and Sustainable Energy Reviews, 60, 41-59.

[7] Maleki, A., Haghighi, A., El Haj Assad, M., Mahariq, I., & Alhuyi Nazari, M. (2020). A review on the approaches employed for cooling PV cells. Solar Energy, 209, 170–185.

[8] Arianmehr, I., Ting, D. S. K., Ray, S. (2013). Assisted turbulence convective heat transfer for cooling the photovoltaic cells. ASME 2013, Heat Transfer Summer Conf. Collocated with the ASME 2013 7th International Conference on Energy Sustainability and the ASME 2013 11th International Conference on Fuel Cell Science, Engineering and Technology, Minnesota, United States of America, Publisher: New York : American Society of Mechanical Engineers, 1-10.

[9] Jacobi, A. M., Shah, R. K. (1995). Heat transfer surface enhancement through the use of longitudinal vortices: A review of recent progress. Experimental Thermal and Fluid Science, 11(3), 295-309.

[10] Wu, H., Ting, D. S. K., Ray, S. (2018). The effect of delta winglet attack angle on the heat transfer performance of a flat surface. International Journal of Heat and Mass Transfer, 120, 117–126.

[11] da Silva, F. A. S., Dezan, D. J., Pantaleão, A. V., Salviano, L. O. (2019). Longitudinal vortex generator applied to heat transfer enhancement of a flat plate solar water heater. Applied Thermal Engineering, 158, 113790.

[12] Naik, H., & Tiwari, S. (2018). Effect of Rectangular Winglet Pair in Common Flow Down Configuration on Heat Transfer from an Isothermally Heated Plate. Heat Transfer Engineering, 39(20), 1778–1793.

[13] Lei, Y. G., He, Y. L., Tian, L. T., Chu, P., Tao, W. Q. (2010). Hydrodynamics and heat transfer characteristics of a novel heat exchanger with delta-winglet vortex generators. Chemical Engineering Science, 65 (5), 1551-1562.

[14] Wijayanta, A. T., Yaningsih, I., Aziz, M., Miyazaki, T., Koyama, S. (2018). Double-sided delta-wing tape inserts to enhance convective heat transfer and fluid flow characteristics of a double-pipe heat exchanger. Applied Thermal Engineering, 145, 27-37.

[15] Hiravennavar, S. R., Tulapurkara, E. G., Biswas, G. (2007). A note on the flow and heat transfer enhancement in a channel with built-in winglet pair. International Journal of Heat and Fluid Flow, 28 (2), 299-305.

[16] Althaher, M. A., Abdul-Rassol, A. A., Ahmed, H. E., Mohammed, H. A. (2012). Turbulent heat transfer enhancement in a triangular duct using delta-winglet vortex generators. Heat Transfer - Asian Research, 41(1), 43–62.

[17] Tang, L. H., Chu, W. X., Ahmed, N., Zeng, M. (2016). A new configuration of winglet longitudinal vortex generator to enhance heat transfer in a rectangular channel. Applied Thermal Engineering, 104, 74-84.

[18] Sinha, A., Chattopadhyay, H., Iyengar, A. K., Biswas, G. (2016). Enhancement of heat transfer in a fin-tube heat exchanger using rectangular winglet type vortex generators. International Journal of Heat and Mass Transfer, 101, 667–681.

[19] Pourhedayat, S., Pesteei, S. M., Ghalinghie, H. E., Hashemian, M., Ashraf, M. A. (2020). Thermal-exergetic behavior of triangular vortex generators through the cylindrical tubes. International Journal of Heat and Mass Transfer, 151, 119406.

[20] Abdollahi, A., Shams, M. (2015). Optimization of shape and angle of attack of winglet vortex generator in a rectangular channel for heat transfer enhancement. Applied Thermal Engineering, 81, 376-387.

[21] Salviano, L. O., Dezan, D. J., Yanagihara, J. I. (2015). Optimization of winglet-type vortex generator positions and angles in plate-fin compact heat exchanger: Response Surface Methodology and Direct Optimization. International Journal of Heat and Mass Transfer, 82, 373-387.

[22] Thermal Conductivity of Selected Materials and Gases. Retrieved January 28, 2021, https://www.engineeringtoolbox.com/thermal-conductivity-d_429.html.

[23] Emissivity Coefficient Materials. Retrieved January 28, 2021, from https://www.engineeringtoolbox.com/emissivity-coefficients-d_447.html.

[24] Tennekes, H. (Hendrik), Lumley, J. L. (1972). A first course in turbulence. Cambridge, Mass: MIT Press.

[25] Radiation Heat Transfer. Retrieved January 28, 2021, from https://www.engineeringtoolbox.com/radiation-heat-transfer-d_431.html.

[26] Jørgensen, F. E. (2005). How to Measure Turbulence with Hot-Wire Anemometers: A Practical Guide, Dantec dynamics, Denmark, 1-56.

[27] Ting, D. S-K. (2016). Basics of Engineering Turbulence, Academic Press, New York.

[28] Taylor, G. I (1938). The spectrum of turbulence, Proceedings of the Royal Society of London. Series A, Mathematical and Physical Sciences, 164, 476-490.

[29] Figliola, R. S. Beasley, D. E. (2011). Theory and Design for Mechanical Measurements, 5th ed, John Wiley & Sons Inc, United States of America.

[30] Myers, J. L., Well, A., Lorch, R. F. (2010). Research design and statistical analysis. 3rd ed, Routledge, New York.

[31] Luo, L., Wen, F., Wang, L., Sundén, B., Wang, S. (2017). On the solar receiver thermal enhancement by using the dimple combined with delta winglet vortex generator. Applied Thermal Engineering, 111, 586-598.

[32] Yang, Y., Ting, D. S. K., & Ray, S. (2020). Heat transfer enhancement of a heated flat surface via a flexible strip pair. International Journal of Heat and Mass Transfer, 159, 120139.

[33] Sun, Z., Zhang, K., Li, W., Chen, Q., Zheng, N. (2020). Investigations of the turbulent thermal-hydraulic performance in circular heat exchanger tubes with multiple rectangular winglet vortex generators. Applied Thermal Engineering, 168, 114838.

[34] Wu, J. (2006). Numerical investigation and analysis of the heat transfer enhancement in channel by longitudinal vortex based on the field synergy principle. Hsi-An Chiao Tung Ta Hsueh/Journal of Xi'an Jiaotong University, 40(9), 996–1000.

CHAPTER 3

CONCLUSIONS & RECOMMENDATIONS

3.1 Summary and Conclusions

This study experimentally investigates the role of the transverse distance between the trailing edges of the winglet pair (D=0, D=1h & D=2h) at Re_h=6300 on heat transfer and flow characteristics. The chosen winglet attack angle is 30°, and chord length and height are 30 mm and 15 mm respectively leading to the aspect ratio (c/h) of 2. Section 2.4.1. investigates the role of transverse distance (D) between the trailing edges of the winglet pair on heat transfer for four cases, D=0, D=1h, D=2h, and D=3h. The D=2h pair optimally-spaced delta winglets consistently resulted in the most potent heat transfer augmentation in terms of maximum peak Nu/Nu_0 over an extended stretch of surface and highest average Nusselt number, $Nu_{avg}/Nu_{0,avg,}$ over the entire tested surface.

The flow characteristics are delineated in Section 2.4.2., for three cases of transverse distance between the trailing edges of the winglet pair viz, D=0, 1h and 2h with the help of hot-wire measurement and from the experimental study, it is revealed that:

- The proximity of the vortices leads to a low velocity contour region of 0.6 and it roughly coincided with maximum turbulent intensity contour zone of 0.11, accompanied by the maximum integral scale contour region of 0.9 and minimum Taylor microscale contour region of 0.15.

- As the faster moving fluid approaches the hot surface, the cooling becomes more effective as the fluid is more turbulent near the surface. In other words, the thinning of the boundary layer contributed to the increasing Nu/Nu_0 as D increased from 0 to $2h$.

- Increasing the transverse distance from D=1h to 2h resulted in more cold air towards the hot plate at more negative $\overline{W}/U_\infty$ region and more hot air scooped away from the plate at the more positive $\overline{W}/U_\infty$ region. It appears that a significant inflow followed by an equally significant outflow makes heat transfer more effective.

Multiple linear regression analysis considering cross-stream vorticity, Ω, stream-wise time-averaged velocity, $\overline{U}/U_\infty$, vertical time-averaged velocity, $\overline{W}/U_\infty$, stream-wise turbulence intensity, u_{rms}/U_∞, span-wise turbulence intensity, v_{rms}/U_∞, height-wise turbulence intensity, w_{rms}/U_∞, streamwise integral scale, Λ/h, and streamwise Taylor microscale, λ/h, with respect to the normalized Nusselt number, Nu/Nu_0, was performed. The analysis demonstrated that turbulent fluctuation vertically into and out of the plate (boundary layer) as defined by w_{rms}/U_∞ has the largest influence on the heat transfer enhancement. The second most influential flow parameter is the stream-wise velocity, $\overline{U}/U_\infty$, which is responsible for moving the incoming air over the plate. Over the range of studied conditions, the velocity perpendicular to the plate, $\overline{W}/U_\infty$ that brings in freestream cool air into the hot plate has the third largest impact on the heat transfer rate. Ranking fourth is the stream-wise turbulence intensity, u_{rms}/U_∞, which is less than 60% as influential as its normal-to-the-plate counterpart w_{rms}/U_∞. The D=2h winglet pair

furnished the largest values of these most effectual flow parameters primarily via a pair of vibrant counter-rotating vortex streets that are closest to the plate.

3.2 Recommendations

The delta winglets are promising turbulent generators in enhancing convective heat transfer. The 2*h*-spaced winglets can effectively contribute to heat transfer augmentation. This study includes the Nu/Nu_0 over an extended stretch of surface and highest average Nusselt number, $Nu_{avg}/Nu_{0,\,avg,}$ over the entire tested surface for 3*h* spaced winglets. The flow characteristics of the 3*h* spaced winglets can be studied to support the current heat transfer results.

Other parameters of the winglets such as size of the winglets can be scrutinized. Winglets with much larger height cause increase in Reynolds number as the Reynolds number is based on height, while the wind speed is constant. Other way round, the wind speed can also be increased, keeping the dimensions of the winglet constant. These can have a different influence on heat transfer. A row of winglets can be studied before implementing the winglets into practical application.

APPENDICES

Appendix A. Uncertainty Analysis

Uncertainty Analysis

The total uncertainty, *E*, consisted by the bias (*B*) and precision (*P*) uncertainties [1],

$$E = \sqrt{B^2 + P^2} \tag{A-1}$$

Uncertainty of U_i

At characteristic point of *Y/h*=0 and *Z/h*=1.5, the bias uncertainty of instantaneous velocity was influenced by the process of calibration (0.194 m/s), linearization (0.097 m/s), A/D resolution (0.078 m/s), and probe positioning (0.015 m/s). The bias uncertainty of the instantaneous velocities was thus approximately,

$$B(U_i) = \sqrt{0.194^2 + 0.097^2 + 0.078^2 + 0.015^2} = 0.2\ \mathrm{m/s} \tag{A-2}$$

We rested the hotwire to freestream and measured the velocity 20 times and thus provided an estimate of the precision uncertainty. For every measurement, $N = 10^6$ points were recorded, and precision, *P*, was assumed to follow the Student's distribution method with a confidence interval of 95%, giving

$$P(U_i) = 0.11\ \mathrm{m/s} \tag{A-3}$$

Then the total uncertainty of U_i was thus

$$E(U_i) = \sqrt{B(U_i)^2 + P(U_i)^2} = \sqrt{0.20^2 + 0.11^2} = 0.23\ \mathrm{m/s} \tag{A-4}$$

Uncertainty of $\overline{U}$, $\overline{V}$, & $\overline{W}$

For the mean velocity (7 m/s), the bias uncertainty was assumed to have the same value as the bias uncertainty of the instantaneous velocity,

$$B(\bar{U}) = B(U_i) = 0.20 \text{ m/s} \quad \text{(A-5)}$$

The precision uncertainty of the mean velocity was obtained by resetting the hotwire to the typical position and measuring the velocity for 20 times. The resulting precision of $\bar{U}$,

$$P(\bar{U}) = 0.20 \text{ m/s} \quad \text{(A-6)}$$

From the above equations, the total uncertainty of $\bar{U}$ was obtained to be,

$$E(\bar{U}) = \sqrt{B(\bar{U})^2 + P(\bar{U})^2} = \sqrt{0.20^2 + 0.20^2} = 0.28 \text{ m/s},$$
$$E(\bar{V}) = 0.021 \text{ m/s}, \; E(\bar{W}) = 0.021 \text{m/s} \quad \text{(A-7)}$$

Uncertainty of u_{rms}, v_{rms}, & w_{rms}

We estimated the bias uncertainty in u_{rms} to be,

$$B(u_{rms}) = 0.010 \text{ m/s} \quad \text{(A-8)}$$

Based on 20 repeated measurements, we estimated the precision of u_{rms},

$$P(u_{rms}) = 0.028 \text{ m/s} \quad \text{(A-9)}$$

The total uncertainty of u_{rms}, v_{rms}, w_{rms} were calculated to be, respectively,

$$E(u_{rms}) = \sqrt{B(u_{rms})^2 + P(u_{rms})^2} = \sqrt{0.01035^2 + 0.028^2} = 0.029 \text{ m/s} \quad \text{(A-10)}$$
$$E(v_{rms}) = \sqrt{\mathrm{B}(v_{rms})^2 + P(v_{rms})^2} = \sqrt{0.01035^2 + 0.025^2} = 0.026 \text{ m/s} \quad \text{(A-11)}$$
$$E(w_{rms}) = \sqrt{B(w_{rms})^2 + P(w_{rms})^2} = \sqrt{0.01035^2 + 0.021^2} = 0.023 \text{ m/s} \quad \text{(A-12)}$$

Heat Transfer

We captured the temperature distribution using a thermal camera calibrated by a thermocouple having a bias uncertainty of 0.5℃. Based on 10 repeated surface temperature measurements, we estimated a precision uncertainty of 0.36℃. Using the propagation of the uncertainty, each parameter's uncertainty involved in the heat transfer was estimated using,

$$E(\dot{Q}_{Total}) = \sqrt{[\frac{\partial \dot{Q}_{Total} E(T_{Top})}{\partial T_{Top}}]^2} = \frac{K_{PTFE} A}{t_{PTFE}} E(T_{Top}) \quad \text{(A-11)}$$

$$E\left(\dot{Q}_{radiation}\right) = \sqrt{\left[\frac{\partial \dot{Q}_{radiation} E(T_{Top})}{\partial T_{Top}}\right]^2} = 4\varepsilon\sigma A T_{Top}^3 E(T_{Top}) \quad \text{(A-12)}$$

$$E\left(\dot{Q}_{convection}\right) = \sqrt{\left[\frac{\partial \dot{Q}_{convection} E\left(\dot{Q}_{Total}\right)}{\partial \dot{Q}_{Total}}\right]^2 + \left[\frac{\partial \dot{Q}_{radiation} E\left(\dot{Q}_{radiation}\right)}{\partial \dot{Q}_{radiation}}\right]^2}$$

$$E\left(\dot{Q}_{convection}\right) = \sqrt{[E(\dot{Q}_{Total})]^2 + [E(\dot{Q}_{radiation})]^2} \quad \text{(A-13)}$$

$$E\left(\dot{h}_{convection}\right) = \sqrt{\left[\frac{\partial hE(\dot{Q}_{convection})}{\partial \dot{Q}_{convection}}\right]^2 + \left[\frac{\partial hE(T_{Top})}{\partial T_{Top}}\right]^2}$$

$$E\left(\dot{h}_{convection}\right) = \sqrt{\left[\frac{E(\dot{Q}_{convection})}{A(T_{Top} - T_{air})^2}\right]^2 + \left[\frac{\dot{Q}_{convection} E(T_{Top})}{A(T_{Top} - T_{air})^2}\right]^2} \quad \text{(A-14)}$$

$$E\left(\frac{Nu}{Nu_0}\right) = \frac{E(\dot{h}_{convection})}{E(\dot{h}_{convection,0})} \quad \text{(A-15)}$$

According to calibration error [1] and Equations A-11 to A-15, the uncertainty of Nu/Nu_0 was found to be 0.061. Moreover, we estimated the uncertainty in probe positioning to be around 0.2*h*. Uncertainty of thermocouple was 0.5℃ and the thermal camera was 0.36℃. According to Ref [1], the uncertainty of each parameter considered in this study was calculated. Table A.1 tabulates the uncertainties of mean velocities and their respective root-mean squares uncertainties, and Table A.2 tabulates the representative uncertainties of all the studied parameters.

Table A.1. Typical uncertainties of mean velocities and their respective root-mean squares uncertainties.

Parameter	$\bar{U}$	$\bar{V}$	$\bar{W}$	u_{rms}	v_{rms}	w_{rms}
Uncertainty	0.28	0.021	0.021	0.029	0.026	0.023

Table A.2. Representative uncertainties of studied parameters

Parameter	$\frac{Nu}{Nu_0}$	$\frac{\bar{U}}{U_\infty}$	$\frac{\bar{V}}{U_\infty}$	$\frac{\bar{W}}{U_\infty}$	Ω
Uncertainty	0.061	0.040	0.003	0.003	0.004
Parameter	$\frac{u_{rms}}{U_\infty}$	$\frac{v_{rms}}{U_\infty}$	$\frac{w_{rms}}{U_\infty}$	$\frac{\Lambda}{h}$	$\frac{\lambda}{h}$
Uncertainty	0.004	0.0037	0.0033	0.04	0.004

References

[1] Figliola, R. S. Beasley, D. E. (2011). Theory and Design for Mechanical Measurements, 5th ed, John Wiley & Sons Inc, United States of America.

Appendix B. Turbulent Intensity & Stream-wise Normalized Velocity, $\bar{U}/U_\infty$, of Inflow, Outflow, and Base Flat Plate Case

The comparison of u_{rms}/U_∞, v_{rms}/U_∞, and w_{rms}/U_∞ at 10h downstream for the 2h-spaced winglets pair is shown in Figure B.1. The uncertainty in u_{rms}/U_∞, v_{rms}/U_∞, and w_{rms}/U_∞ were estimated to be around 0.004, 0.0037, and 0.0033, respectively. The inflow and outflow regions are chosen from the Figure 2.6, chapter 2, section 2.4.2.1, where the arrows point downwards (upwards) represents inflow (outflow) and at the location of Y/h = -2.0, and -0.5, for inflow and outflow, respectively. It is noted that w_{rms}/U_∞ at inflow is larger than the outflow region near the surface. This seems to be useful for differentiating the inflow and outflow regions when compared to the vorticity (Ω). In other words, the normalized vertical velocity, $\bar{W}/U_\infty$, acts as an important parameter to clearly differentiate inflow and outflow. Note that the high turbulent intensity can significantly contribute to heat transfer. The turbulent intensities for all three components are almost similar, with a largest difference among u_{rms}/U_∞, v_{rms}/U_∞, w_{rms}/U_∞ being only 3% at same location. It is also noted that both at inflow and outflow the W component turbulent intensity values are higher near the surface and as the normal distance from the plate is increased, the U component turbulent intensity values become higher at the proximity of vortex core area signifying both the U and W components turbulent intensities are significant in contributing to heat transfer compared to V component. In Figures 2.9 from chapter 2, the maximum turbulence intensity of 0.096, 0.11, & 0.11 is obtained nearly in the vortex regions of Y/h= -1.0 & Z/h=1.25, Y/h= -1.75 & Z/h=1.25, Y/h= -2.25 & Z/h= 1.0, respectively. And this turbulence intensity decreases apart from the proximity of the solid surface to the

freestream regions near both inflow and outflow regions. This confirms the low background turbulence outside the boundary layers near the freestream area.

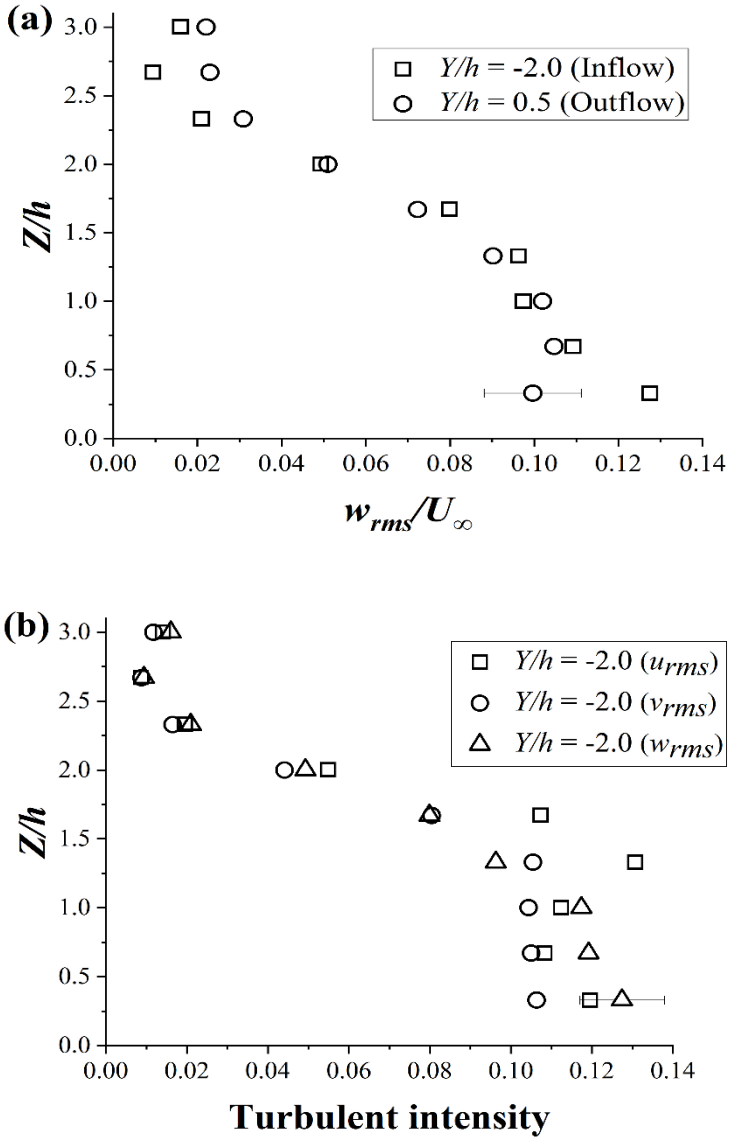

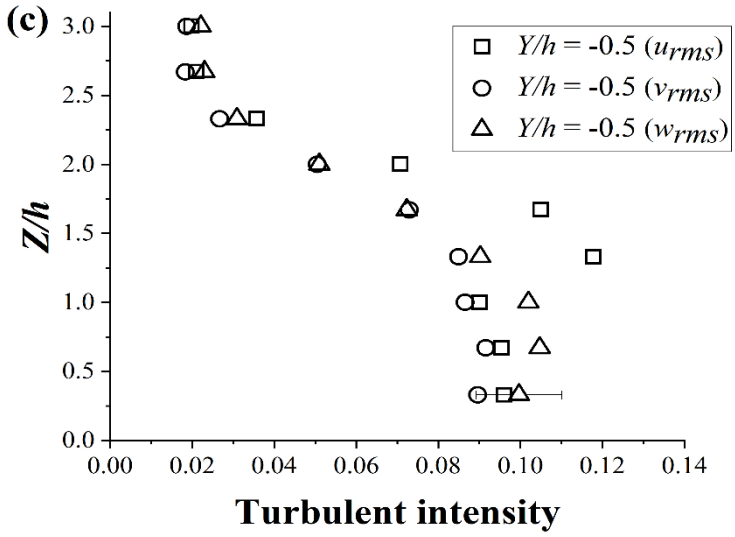

Figure B.1. Turbulent intensities (u_{rms}/U_∞, v_{rms}/U_∞, and w_{rms}/U_∞) at inflow and outflow regions at 10*h* downstream of the 2*h*-spaced winglet pair.

The comparison of v_{rms}/U_∞, and w_{rms}/U_∞ at 10*h* distance downstream for the 2*h*-spaced winglets pair is shown in Figure B.2. The uncertainty in v_{rms}/U_∞, and w_{rms}/U_∞ were estimated to be 0.0037, and 0.0033, respectively. It is clear from Figure B.2(a) that as the fluid approaches the surface the turbulence intensity increases. It is also noted that the near-surface turbulent intensity is higher at inflow and outflow region which can be seen in Figure B.2(b), and this roughly coincides with the increase in Nu/Nu_0, making D=2*h* case superior compared to D=0 and D=1*h* cases.

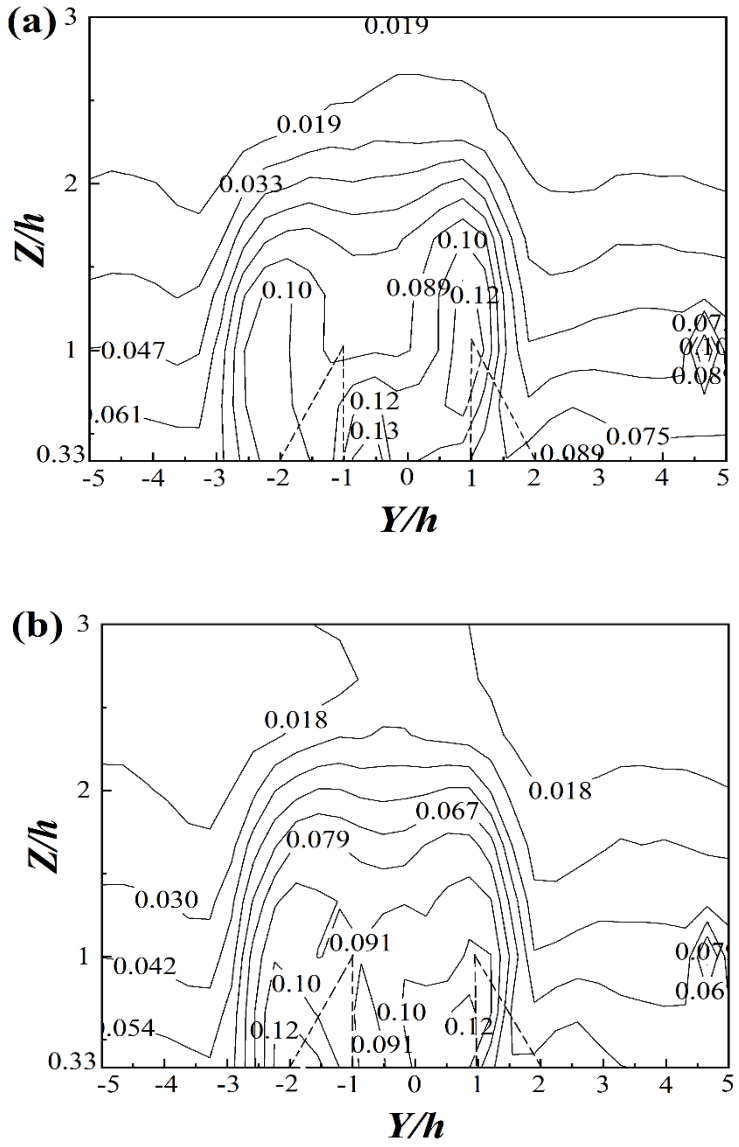

Figure B.2. (a) Spanwise turbulent intensity contours (v_{rms}/U_∞) and (b) height wise turbulent intensity contours (w_{rms}/U_∞) in the *YZ* plane at 10*h* downstream for 2*h* spaced winglet pair.

Figure B.3 shows the stream-wise normalized velocity, $\overline{U}/U_\infty$, of inflow, outflow, and base flat plate case (without winglets) at *X*=10*h* downstream distance for 2*h*-spaced winglet pair. Boundary layer thickness is the location of the height where the *U* component velocity is 99% of freestream velocity. For flat plate without winglets the

boundary layer lies approximately near 6 mm (0.33*h*) at 10*h* downstream of the winglet [1]. The turbulent boundary layer can be derived from $\frac{\delta}{h} = \frac{0.37}{Re_h^{1/5}}$ and it is around 5.7mm, where δ is the boundary layer thickness, *h* is the winglet height and Re_h is the Reynolds number based on winglet height. The inflow and outflow regions are chosen from chapter 2, section 2.4.2.1, Figure 2.6, where the arrows point downwards (upwards) represents inflow (outflow) and this correspond to the location of *Y/h* = -2.0, 1.5, and -0.5, 0, respectively. The $\bar{U}/U_\infty$ values shown in the Figure B.3 are average of the two inflow and two outflow regions, respectively. The boundary layer is thicker near the inflow region than the outflow. If the normalized velocity near the plate is observed, it is nearly 0.8 at inflow which is significantly higher than the base plate of 0.76 contributing to better heat transfer. Near the plate, the outflow region is 0.66 and heat transfer is expected to be less at this region.

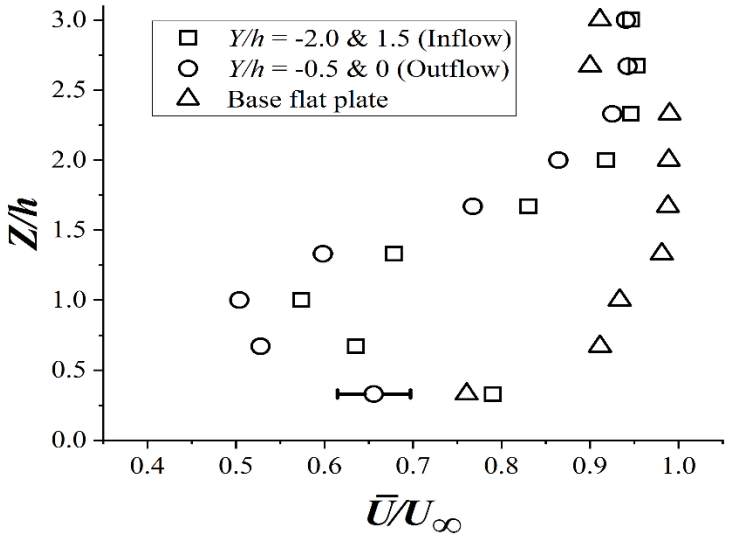

Figure B.3. Stream-wise normalized velocity $\bar{U}/U_\infty$ of inflow, outflow, and base flat plate case at *X*=10*h* downstream distance of the D=2*h* winglet pair.

References

[1] Gerhart P. M., Gerhart A. L., Hochstein J. I., Munson, Young, Okiishi's (2016). Fundamentals of Fluid Mechanics, eighth ed.,Wiley, New York.

Appendix C. Impact of Individual Flow Parameters on Heat Transfer

The impact of cross-stream dimensionless vorticity (Ω), stream-wise time-averaged velocity normalized by U_∞ ($\bar{U}/U_\infty$), vertical averaged $\bar{W}/U_\infty$, stream-wise turbulence intensity normalized by freestream time-averaged velocity (u_{rms}/U_∞), span-wise turbulence intensity normalized by freestream time-averaged velocity (v_{rms}/U_∞), height-wise turbulence intensity normalized by freestream time-averaged velocity (w_{rms}/U_∞), integral scale normalized by winglet height (Λ/h), and Taylor microscale normalized by winglet height (λ/h) on heat transfer enhancement (Nu/Nu_0) at a downstream distance of X=10h, spanwise distance of Y=±3h, and at Z=0.33h is shown in Figure C.1 starting from the parameter which had lower influence to the parameter which had higher influence on heat transfer according to multiple linear regression results shown in Chapter 2, Section 2.4.3. The correlations of studied flow parameters and Nu/Nu_0 appear similarly scattered, still we can see that certain flow parameters correlate better with the heat transfer enhancement than others. The significant scatter is primarily because every data point corresponds a condition where the values of the different flow parameters are unique to that data point. For example, when correlating Nu/Nu_0 with $\bar{W}/U_\infty$ in Figure C.1(f) for D=1h case, the data points correspond to changes in w_{rms}/U_∞, $\bar{U}/U_\infty$, and others, in addition to variation in $\bar{W}/U_\infty$. It is found that the height-wise turbulent intensity normalized by time-averaged free-stream velocity (w_{rms}/U_∞) has most significant impact on heat transfer as the turbulent intensity near the surface is larger compared to the other areas and the high Nu/Nu_0 values corresponds to the high turbulent intensity locations for 2h-spaced winglets. The impact of stream-wise velocity normalized by time-averaged free-stream velocity ($\bar{U}/U_\infty$) also has significant impact on

Nu/Nu_0. The higher stream-wise velocity locations compared to the base case (without winglets) denotes the inflow region and this roughly coincide with high Nu/Nu_0 and these locations are outnumbered by 2*h*-spaced winglets than other cases. Next to stream-wise velocity, the vertical velocity towards the hot surface normalized by time-averaged free-stream velocity ($\bar{W}/U_\infty$) has marginal effect on Nu/Nu_0. The $\bar{W}/U_\infty$ has both negative values (inflow) and positive values (outflow). The 2*h*-spaced winglets have significant lowest negative value and equally significant positive value denoting that the vortices generated by 2*h*-spaced winglets are more organized making significant impact on heat transfer. The higher fluctuation of both streamwise velocity, u_{rms}/U_∞, and cross-stream turbulent fluctuation, v_{rms}/U_∞, is beneficial for heat transfer. The magnitude of the cross-stream vorticity, Ω, has a relatively small impact. Recall that we have utilized only the next-to-the-surface data points, and that vorticity is highest at the core of the organized vortices that are somewhat away from the plate. Around the edge of a vortex the vorticity is low. The effects of Λ/h and λ/h are not obvious. Increase in integral length, which implies weaker turbulence, and a negative impact on heat transfer. Taylor microscale, λ/h, seems to convey that when an eddy is large, it negatively influences the heat transfer.

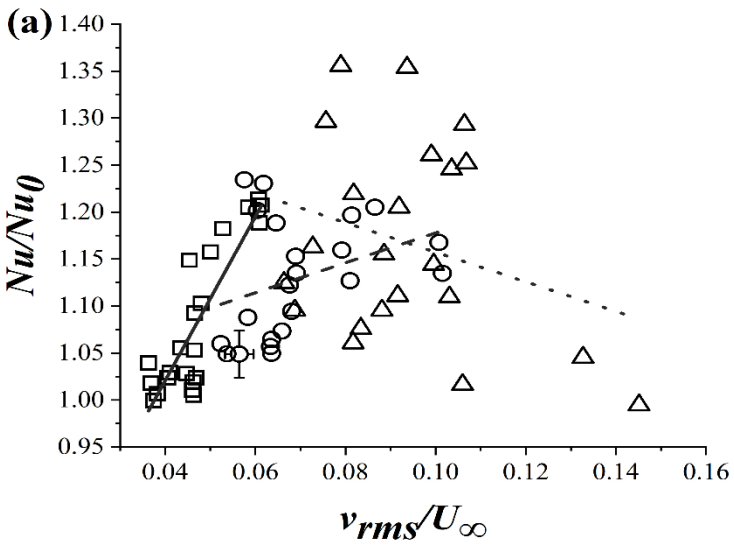
(a)
1.40
1.35
1.30
1.25
1.20
1.15
1.10
1.05
1.00
0.95
Nu/Nu0
0.04
0.06
0.08
0.10
0.12
0.14
0.16
vrms/U∞

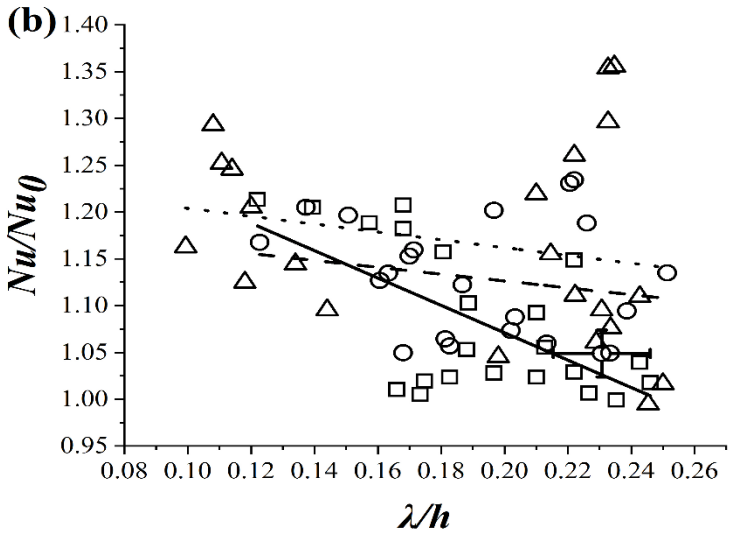
(b)
1.40
1.35
1.30
1.25
1.20
1.15
1.10
1.05
1.00
0.95
Nu/Nu0
0.08
0.10
0.12
0.14
0.16
0.18
0.20
0.22
0.24
0.26
λ/h

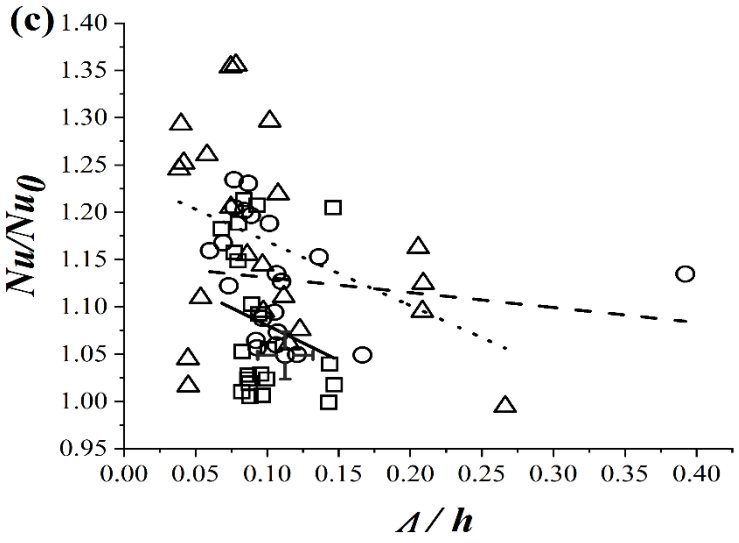
(c)
Nu/Nu0
1.40
1.35
1.30
1.25
1.20
1.15
1.10
1.05
1.00
0.95
0.00
0.05
0.10
0.15
0.20
0.25
0.30
0.35
0.40
Λ / h

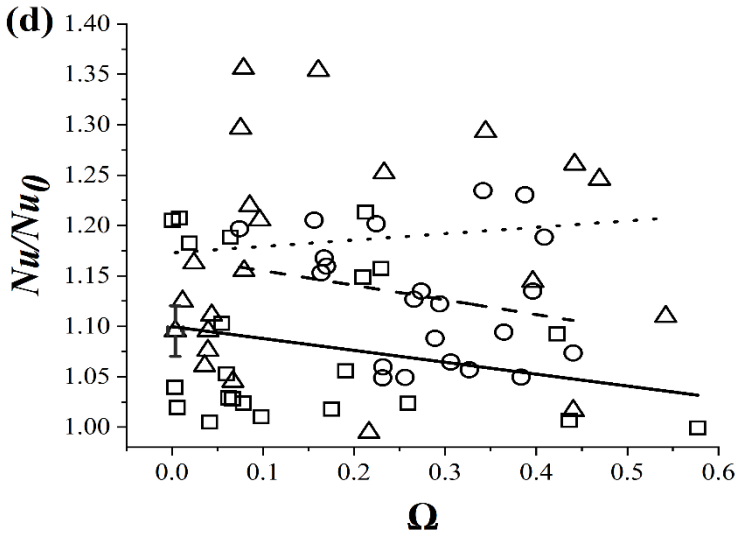
(d)
Nu/Nu0
1.40
1.35
1.30
1.25
1.20
1.15
1.10
1.05
1.00
0.0
0.1
0.2
0.3
0.4
0.5
0.6
Ω

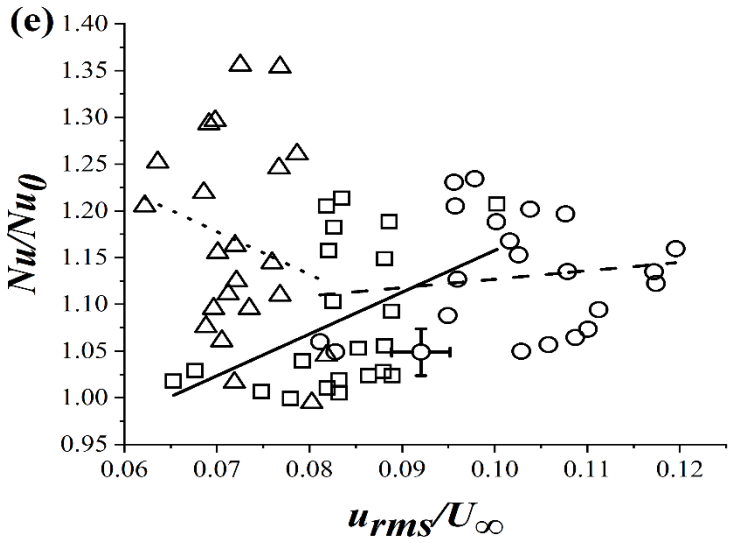
(e)
1.40
1.35
1.30
1.25
1.20
1.15
1.10
1.05
1.00
0.95
Nu/Nu0
0.06
0.07
0.08
0.09
0.10
0.11
0.12
urms/U∞

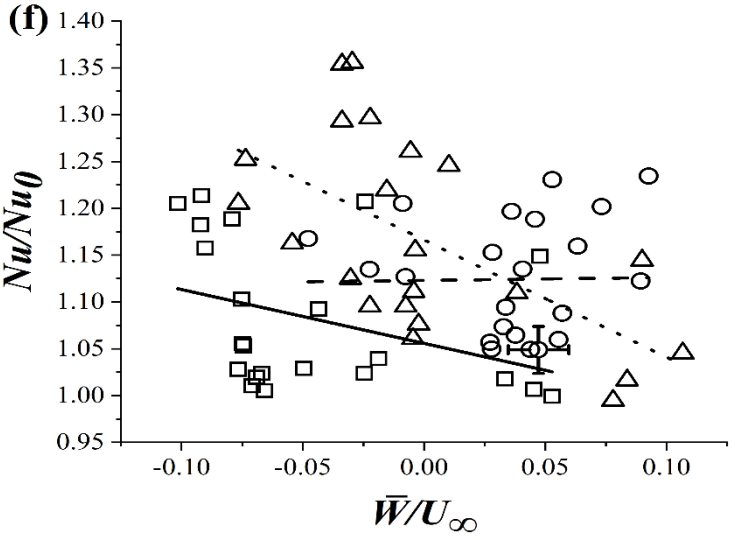
(f)
1.40
1.35
1.30
1.25
1.20
1.15
1.10
1.05
1.00
0.95
Nu/Nu0
-0.10
-0.05
0.00
0.05
0.10
W̄/U∞

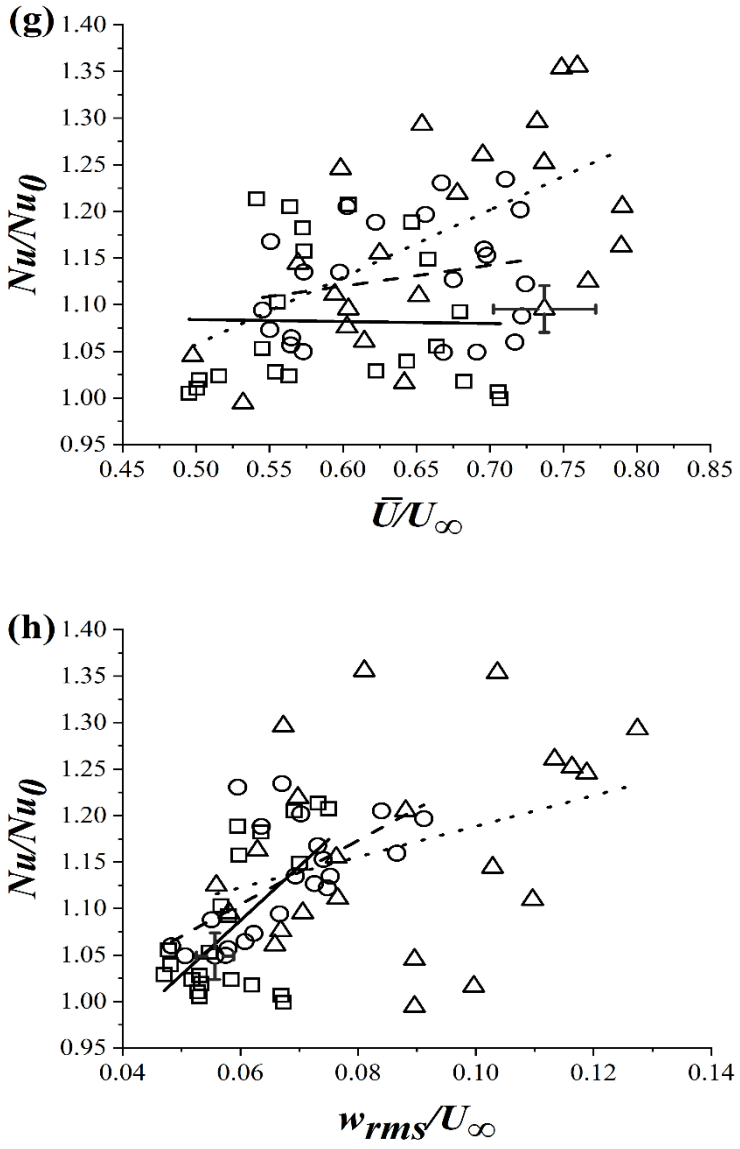

Figure C.1. Correlating normalized, (a) span-wise turbulence intensity, v_{rms}/U_∞, (b) integral scale normalized by winglet height, Λ/h, and (c) Taylor microscale normalized by winglet height, λ/h, (d) cross-stream dimensionless vorticity (Ω), normalized (e) stream-wise turbulence intensity, u_{rms}/U_∞, (f) vertical velocity, $\bar{W}/U_\infty$, (g) stream-wise velocity, $\bar{U}/U_\infty$, (h) height-wise turbulence intensity, w_{rms}/U_∞, with Nu/Nu_0 at X=10h, Y=±3h, and Z=0.33h. The solid, dashed and dotted lines represent the linear fits for D=0, D=1h and D=2h cases, respectively. R-square values of v_{rms}/U_∞ are 0.74275, 0.12041, &

0.08104 for 0, 1h and 2h spaced winglets, respectively. R-square values of λ/h are 0.38644, 0.0411, & 0.0489 for 0, 1h and 2h spaced winglets, respectively. R-square values of Λ/h are 0.052. 0.02836, & 0.16783 for 0, 1h and 2h spaced winglets, respectively. R-square values of Ω are 0.00034, 0.05518, & 0.33887 for 0, 1h and 2h spaced winglets, respectively. R-square values of u_{rms}/U_∞ are 0.18005, 0.02096, & 0.04513 for 0, 1h and 2h spaced winglets, respectively. R-square values of $\overline{W}/U_\infty$ are 0.13115, 0.0022, & 0.35856 for 0, 1h and 2h spaced winglets, respectively. R-square values of $\overline{U}/U_\infty$ are 0.00034, 0.05518, & 0.58213 for 0, 1h and 2h spaced winglets, respectively. R-square values of w_{rms}/U_∞ are 0.38449. 0.38470, & 0.1141 for 0, 1h and 2h spaced winglets, respectively.

Appendix D. Impact of Non-ideal Real Wind Effects

The hourly average wind speed and most frequent wind direction for the period 1981 to 2010 in Windsor is obtained to be 15.5 km/hr (4.3 m/s) and south-west direction, respectively [1]. From the data provided by Ref [1], the standard deviation of hourly wind speed is calculated to be 2.45 m/s. From this the wind turbulence can be calculated by dividing the standard deviation of hourly wind speed by the average hourly wind speed (4.3 m/s). The corresponding wind turbulence is calculated to be around 0.16. According to Althaher et al. [2], as the Reynolds number increases, the base Nusselt number increases by using delta winglets pairs. They varied the Reynolds number based on mean velocity variation indicating that the increase in mean wind velocity can results in increased Nusselt number (*Nu*). The wind flow in Windsor has its natural turbulence of 0.16 for an average velocity of 4.3 m/s. This when passes through the delta winglets model proposed in this study can cause a raise in turbulence and considered the increase in wind velocity, it would be beneficial for effective fluid mixing thereby increasing the local Nusselt number and helps in enhancing the heat transfer from the hot surface.

References

[1] *Canadian Climate Normals 1981-2010 Station Data - Climate - Environment and Climate Change Canada*. (n.d.). Retrieved January 8, 2021, from https://climate.weather.gc.ca/climate_normals/results_1981_2010_e.html?searchType=stnName&txtStationName=Windsor&searchMethod=contains&txtCentralLatMin=0&txtCentralLatSec=0&txtCentralLongMin=0&txtCentralLongSec=0&stnID=4716&dispBack=0

[2] Althaher, M. A., Abdul-Rassol, A. A., Ahmed, H. E., Mohammed, H. A. (2012). Turbulent heat transfer enhancement in a triangular duct using delta-winglet vortex generators. Heat Transfer - Asian Research, 41(1), 43–62.

Appendix E. Dimensional Analysis and Scaling Factor for Winglets

The results shown in this work are in non-dimensional form. All the heat transfer and flow characteristics results are normalized by the height of the winglet (h=15 mm). The longitudinal vortices survived till the downstream distance of 20h i.e., 300 mm of the heated plate for the winglet height of 15 mm. If these winglets are practically needing to be implanted in a solar panel of 1-meter length, then approximately winglets with height of 50mm are needed. Accordingly, the chord length also needed to be scaled up to 100mm to provide an aspect ratio of 2 to witness the same performance obtained from this study. Increasing the winglet height increases the Reynolds number as it is based on the winglet height and it positively influences the heat transfer as presented in the previous section, Appendix D.

VITA AUCTORIS

NAME:	Siddharth Koushik Mohanakrishnan
PLACE OF BIRTH:	Chennai, India
YEAR OF BIRTH:	1995
EDUCATION:	Anna University, B.E., Chennai, India, 2017
	University of Windsor, M.Sc., Windsor, ON, 2021